1   **Sedimentary organic carbon dynamics in a glaciated Arctic fjord: tracing**

2   **contributions of terrestrial and marine sources in the context of Atlantification**

3   **over recent centuries**

4

5   Dahae Kim[a], Jung-Hyun Kim[a,*], Youngkyu Ahn[a], Matthias Forwick[b], Seung-Il Nam[a]

6

7   [a]Korea Polar Research Institute, 26 Songdomirae-ro, Yeonsu-gu, Incheon 21990, South

8   Korea

9   [b]UiT The Arctic University of Norway, Department of Geosciences, NO-9037 Tromsø,

10   Norway

11

12

13

14   ***Correspondence:**

15   Jung-Hyun Kim (jhkim123@kopri.re.kr)

16

17

18

Abstract

In this study, we investigated sedimentary organic carbon (OC) dynamics in Kongsfjorden, Svalbard, using three multicores collected during the HH22 and HH23 cruises aboard the RV *Helmer Hanssen* in 2022 and 2023. We assessed the relative contributions of petrogenic, soil-derived, plant-derived, and marine OC by applying a four-source apportionment approach based on $\Delta^{14}C_{org}$, $\delta^{13}C_{org}$, and lignin parameters, including the $(Ad/Al)_v$ ratio and lignin phenol concentrations, with Monte Carlo (MC) analysis. Age-depth models based on ^{210}Pb and ^{226}Ra data were used to evaluate temporal variations in the accumulation rates (ARs) of sedimentary OC. Our results revealed a marked increase in marine OC ARs over the past decades, closely linked to enhanced Atlantic Water (AW) inflow. The increasing AW influence in Arctic fjords observed in our record points to the potential for continued Atlantification under Arctic warming, as retreating sea ice and glaciers lower barriers to AW intrusion, enabling deeper and more persistent inflow. By placing this recent AW trend into historical context, our study provides valuable insights into the biogeochemical consequences of ongoing and future climate change in Arctic fjord systems.

1. Introduction

The Arctic region is currently experiencing rapid climate change, with surface air temperatures rising nearly four times faster than the global average since 1979 (Rantanen et al., 2022). This accelerated warming has profound implications for Arctic ecosystems and carbon dynamics (Dahlke et al., 2020; Friedlingstein et al., 2020). Arctic fjords, in particular, are recognized for their high sediment accumulation rates, receiving substantial terrestrial input from glacial meltwater and erosion (Winkelmann and Knies, 2005). As a result, they function as critical hotspots for global organic carbon (OC) burial and serve as high-resolution archives of environmental change (Smith et al., 2015; Bianchi et al., 2020). Given the extreme rates of warming, Arctic fjords are increasingly vulnerable to climate-driven transformations that reflect broader shifts occurring across the Arctic system. While modern observational records provide valuable but temporally constrained insights, sediment cores and other paleoenvironmental archives are essential for reconstructing long-term trends in OC dynamics over the past centuries (Ingrosso et al., 2025).

The high Arctic Svalbard archipelago, a key transitional zone between the North Atlantic and Arctic Oceans, is characterized by widespread glaciation, with approximately 57% of its landmass covered by glaciers (Nuth et al., 2013). A major driver of recent environmental change in this region is the enhanced inflow of warm, saline Atlantic Water (AW) via the West Spitsbergen Current (WSC), which strongly influences the western coast of Spitsbergen, the largest island in the archipelago (De Rovere et al., 2022). This process, termed Atlantification, has intensified over recent decades, accelerating the decline of summer sea ice extent, enhancing tidewater glacier melt, and increasing freshwater discharge into fjords (e.g., Jernas et al., 2018; Krajewska et al., 2020; Skogseth et al., 2020). Kongsfjorden, located on the western coast of Spitsbergen, has emerged as a key site for investigating the impacts of recent Arctic warming due to its dynamic oceanographic regime and sensitivity to AW inflow (e.g., Tesi et al., 2021). Although previous studies have characterized the spatial variability of sedimentary OC in Kongsfjorden using bulk elemental and isotopic parameters (e.g., Winkelmann and Knies, 2005; Kuliński et al., 2014; Kumar et al., 2016) molecular-level assessments of sedimentary OC sources, especially over the past centuries, remain limited.

A recent study by Kim et al. (2023) began addressing this gap by analyzing the sources and composition of surface sedimentary OC across eight Svalbard fjords, including Kongsfjorden. Their findings provided valuable insights into the spatial

74   patterns of contemporary OC dynamics. However, the study did not address the

75   progressive shifts in OC dynamics linked to Atlantification since the mid-1990s, an era

76   marked by intensified AW intrusion and ecosystem change. These longer-term

77   oceanographic transformations have been well-documented (e.g., Årthun et al., 2012;

78   Polyakov et al., 2017; Lind et al., 2018; Tesi et al., 2021) but are not yet fully integrated

79   into our understanding of sedimentary OC in Svalbard fjords. The lack of long-term

80   observational and historical data on AW inflow in this region highlights the urgent need

81   for sedimentary records to establish baselines and quantify rates of environmental change

82   (e.g., Cottier et al., 2007; Tesi et al., 2021; Jordà-Molina et al., 2023). Such records are

83   invaluable for distinguishing between natural variability and human-induced changes,

84   providing insights into the mechanisms driving environmental changes in Arctic fjords.

85   Building on the findings of Kim et al. (2023), this study aimed to generate longer-

86   term reconstructed records to fill the current gap in long-term observational and historical

87   data on AW inflow in this region, through the analysis of three multicores collected along

88   a transect from the inner to the outer Kongsfjorden. The primary objectives were to: (1)

89   characterize spatial patterns of sedimentary OC, (2) estimate temporal variations in the

90   relative contributions of sedimentary OC sources over the past centuries, and (3) assess

91   the impact of human-induced climate variability on environmental conditions. To achieve

92   these aims, we applied a multi-proxy approach that integrates bulk geochemical

93   parameters (carbon and nitrogen contents, stable carbon and radiocarbon isotopes),

94   molecular biomarkers (lignin phenols), and sedimentological measurements (bulk dry

95   density, grain size, and surface area). This integrative framework provides critical insights

96   into the coupling between terrestrial and marine systems, and highlights the sensitivity of

97   Arctic fjord environments to both past and ongoing climate change.

98

99   **2. Regional setting**

100   Kongsfjorden and Krossfjorden form the Kongsfjorden–Krossfjorden fjord system,

101   which opens westward into the Kongsfjordrenna, a submarine glacial trough that incises

102   the continental shelf off northwestern Spitsbergen (Fig. 1; Svendsen et al., 2002). This

103   high-latitude fjord complex spans 78°50′ to 79°30′ N and 11° to 13° E. Kongsfjorden, the

104   southern branch (~20 km long, 4–10 km wide, up to 394 m deep), holds ~29.4 km³ of

105   water, while Krossfjorden, the northern branch (~30 km long, 3–6 km wide, max depth

106   374 m), contains ~25 km³ (Ito and Kudoh, 1997; Svendsen et al., 2002). Kongsfjorden's

107   drainage basin (~1440 km²) is ~80% glaciated (Pramanik et al., 2020), receiving

substantial freshwater and sediment from five tidewater glaciers (Kongsvegen, Kronebreen, Kongsbreen, Conwaybreen, and Blomstrandbreen) and the Bayelva River (Zhu et al., 2016; McGovern et al., 2022).

The absence of a sill at the mouth of Kongfjorden allows intrusions of warm (~6°C), saline, nutrient-rich AW (Svendsen et al., 2002; Cantoni et al., 2020). These intrusions, driven by variability in the WSC and wind-induced shelf processes, typically enter at intermediate depths (~100–200 m), increasing subsurface temperatures and salinities and altering hydrographic structure (Svendsen et al., 2002; Tverberg et al., 2019; De Rovere et al., 2022). This weakens stratification, enhances vertical mixing, and impacts sea ice dynamics, glacier melting, and biogeochemical cycles. When occurring during the productive season, AW intrusions can also stimulate primary productivity by delivering nutrients to the euphotic zone. During periods of weak AW advection, colder, fresher Arctic Water from the East Spitsbergen Current (ESC) dominates, strengthening stratification and promoting a more Arctic-like regime.

In addition to oceanic forcing, glacial meltwater strongly influences fjord hydrography and ecology. Meltwater from tidewater glaciers transports large sediment loads, generating turbid plumes that reduce light penetration and suppress primary productivity, particularly near glacier fronts (Ito and Kudoh, 1997; Svendsen et al., 2002). These inputs also deliver terrestrial organic carbon (OC), including petrogenic OC from eroded bedrock and aged OC from soils. Surface runoff from glacial forefields and surrounding catchments further contributes to sediment and OC input. These effects are sustained by the fjord's long water residence time and limited exchange with the open ocean, which support internal circulation and persistent stratification (Svendsen et al., 2002; Cottier et al., 2005; Tverberg et al., 2019).

3. Materials and methods

3.1 Sample collection

Four surface sediment samples were collected from Kongsfjorden and Krossfjorden during the RV *Helmer Hanssen* cruise (HH23) in 2023 (Fig. 1). Three multicores were recovered from Kongsfjorden, Svalbard, at water depths of 81 m (core HH23-1058MUC, hereafter 1058MUC; 45 cm long), 339 m (core HH22-1161MUC, hereafter 1161MUC; 44 cm long), and 323 m (core HH22-1159MUC, hereafter 1159MUC; 40 cm long) during the RV *Helmer Hanssen* cruises (HH22 and HH23) in 2022 and 2023 (Fig. 1). The cores were retrieved using a multi-corer (KC Denmark model 72.000, with 6 core liners; 11 cm

outer diameter; 10.5 cm inner diameter, and 0.8 m length each). The multicores were sectioned onboard at 0.5 cm intervals down to 2 cm depth, and at 1 cm intervals thereafter and stored at –20 ℃. Subsequently, the samples were freeze-dried for further analysis.

3.2 Sedimentological analysis

To characterize sedimentary properties associated with OC transport and deposition, we analyzed water content, dry bulk density, grain size distribution, and specific surface area. Water content was calculated by determining the weight loss of wet bulk samples after freeze-drying. The dry bulk density of homogenized subsamples was measured using an AccuPyc II 1345 pycnometer (Micromeritics, Georgia, USA) at the Korea Polar Research Institute (KOPRI). The average of three measurements was used for grain density calculations to ensure precision, with an analytical error of less than 0.0032 cm^3 observed when employing the 1 cm^3 chamber. Grain size distribution followed the methodology outlined by Ahn et al. (2024). Approximately 130 mg of freeze-dried, unground subsamples were treated with 5 mL of 35% H_2O_2 to oxidize organic matter. A Mastersizer 3000 laser particle size analyzer (Malvern Panalytical B.V., UK) was used for grain size analysis of bulk sediments at KOPRI. Analytical precision was determined as follows: D(10): 37.5 ± 0.3 μm, D(50): 71.4 ± 0.2 μm, D(90): 104.0 ± 0.0 μm. Specific surface area (SA) measurements were conducted following the method described by Kim et al. (2022). Freeze-dried, unground subsamples were first heated at 350 ℃ to remove organic matter and then cooled gradually over 12 hours to room temperature. Prior to analysis, the samples were degassed at 200℃ for 2 hours under a constant flow of N_2 gas using a Micromeritics FlowPrep 060 Sample Degas System at the Korea Basic Science Institute (KBSI, Jeonju Center). Specific SA was measured with N_2 gas as the adsorbate in a He atmosphere, with an analytical precision within $\pm$ 9%. Instrument performance was verified using Carbon Black (21.0 ± 0.75 m²/g; ISO 9277:2010), a certified reference material provided by Micromeritics.

3.3 Radioisotope analysis

To establish sediment chronology and determine sedimentation rates, freeze-dried and ground subsamples (~5 g) were analyzed for ^{210}Pb and ^{226}Ra activities using gamma spectrometry with a well-type High-Purity Germanium (HPGe) detector at KBSI. The analytical uncertainties averaged 9.6 ± 2.0 mBq/g for ^{210}Pb and 2.7 ± 4.1 mBq/g for ^{226}Ra. Excess ^{210}Pb ($^{210}Pb_{ex}$) activities were calculated by subtracting the ^{226}Ra activity from the

176 total ^{210}Pb (^{210}Pb$_{tot}$) activity, following the approach described by Appleby (1998). The

177 apparent sedimentation rate (cm/yr) was calculated from ^{210}Pb$_{ex}$ with the constant rate of

178 supply (CRS) model (cf. Appleby and Oldfield, 1978) with the following equation:

179

180 $$\text{Apparent sedimentation rate} = -\lambda / b \text{ (cm/yr)} \tag{1}$$

181

182 where λ is the radioisotope decay constant for ^{210}Pb (0.03114 per year), and b is the slope

183 of the regression line.

184

185 **3.4 Bulk elemental and carbon isotope analysis**

186 To determine the content and isotopic composition of OC and to infer its sources,

187 we conducted bulk elemental and carbon isotope analyses, including $\delta^{13}C_{org}$ and $\Delta^{14}C_{org}$.

188 The bulk elemental and carbon isotopic composition were determined using the

189 procedure based on Kim et al. (2023). In brief, total nitrogen (N$_{tot}$) and total organic

190 carbon (TOC) contents, as well as carbon isotopic compositions ($\delta^{13}C_{org}$), were

191 analyzed using an elemental analyzer (Thermo Electron Corporation Flash EA 2000,

192 Thermo Fisher Scientific, Germany) connected to an isotope ratio mass spectrometer

193 (Finnigan Delta Plus, Thermo Fisher Scientific, Germany). TOC and $\delta^{13}C_{org}$ were

194 measured on decalcified samples using 1 M HCl for 24 hours. The $\delta^{13}C_{org}$ values were

195 expressed in delta notation (‰) relative to the Vienna Pee Dee Belemnite (VPDB)

196 standard. The analytical precision was within 0.5 wt. % for carbon, 0.5 wt. % for

197 nitrogen, and 0.5‰ for $\delta^{13}C_{org}$.

198 Sediment samples were pretreated with HCl and NaOH to remove carbonates and

199 humic acids, followed by drying at 60°C. The alkali-insoluble fraction was combusted

200 at 900°C in sealed ampoules with CuO to produce CO_2, which was then purified and

201 converted to graphite following the method of Vogel et al. (1984). Radiocarbon

202 (^{14}C/^{13}C) measurements were performed using accelerator mass spectrometry (AMS)

203 at the Center for Applied Isotope Studies (CAIS), University of Georgia, USA. The

204 radiocarbon results were presented in delta notation ($\Delta^{14}C_{org}$, ‰), as defined by Stuiver

205 and Polach (1977).

206

207 **3.5 Lignin phenol analysis**

208 To trace terrestrial OC inputs, particularly those derived from vascular plants, we

209 analyzed lignin phenols using CuO oxidation followed by gas chromatography-mass

spectrometry. CuO oxidation and subsequent analyses were performed following the procedure described by Kim et al. (2023). In brief, homogenized subsamples (~400 mg) were subjected to alkaline CuO oxidation in the presence of cupric oxide and ammonium iron (II) sulfate hexahydrate. This process was conducted using a Microwave Digestion System (MARS 6 microwave, CEM Corporation, USA) at 150°C for 1.5 hours after adding N_2-purged NaOH solution. After oxidation, a known amount of internal standard (ethyl vanillin) was added to the CuO oxidation products. The resulting products were analyzed at KOPRI using an Agilent 7890B gas chromatograph (GC) coupled to a 5977B Series Mass Selective Detector (MSD) (Agilent Technologies, Santa Clara, CA, USA). Analyses were conducted in single ion monitoring (SIM) mode with a DB1-MS capillary column (30 m × 0.25 mm, 0.25 μm, Agilent J&W). The analytical uncertainty for lignin phenols concentrations, determined through replicate measurements of the same sediment samples, was typically less than 10%. Calibration was performed using commercially available standards.

3.6 Accumulation rates

The accumulation rates (AR) of each OC source in the sediment cores were calculated to investigate OC fluxes over recent timescales. Wet bulk density (WBD) and porosity (PO) were determined using the water content and dry bulk density of the samples, as described by Hamilton (1971). The AR was calculated based on the sedimentation rate (SR), WBD, and PO of each sample, as follows (cf. Gealy, 1971):

$$AR \left(\frac{g/cm^2}{yr}\right) = SR \times \left[WBD - 1.025 \times \left(\frac{PO}{100}\right)\right] \tag{2}$$

As the next step, the ARs of bulk OC were calculated using Equation 2, as follows (cf. Nam, 1997):

$$Bulk\ OC\ AR = (TOC\ of\ sediment\ sample/100) \times AR \tag{3}$$

The ARs of petrogenic, soil-derived, plant-derived, and marine OC were calculated from bulk OC AR using Equation 3, as follows:

242          $AR \text{ of each OC source} = (\text{each OC source fraction}/100) \times \text{bulk OC } AR$ (4)

243

4. Results

4.1 Sediment properties

246   The depth profiles of water content, dry bulk density, grain size distribution, mean
247   grain size, and specific surface area (SA) for the three cores are shown in Fig. 2. Water
248   content displayed distinct trends across the cores. The highest water content was observed
249   at the outermost site (core 1159MUC), ranging from 30.3% to 47.5%, with an average of
250     $38.5 \pm 3.2\%$. At the middle site (core 1161MUC), water content ranged from 31.7% to
251   42.2%, with an average of $35.3 \pm 2.2\%$. The innermost site (core 1058MUC) exhibited
252   the lowest range, from 19.7% to 32.6%, with an average of $27.9 \pm 2.3\%$.

253   Dry bulk density measurements showed a decreasing trend from the innermost to the
254   outermost core. Core 1058MUC had a dry bulk density ranging from 2.74 g/cc to 2.77
255   g/cc, for core 1161MUC, the range was 2.68 g/cc to 2.80 g/cc. For core 1159MUC, the
256   range was 2.60 g/cc to 2.69 g/cc.

257   In general, silt content was predominant in all three cores, with the highest average
258   observed at the innermost site (core 1058MUC), where it reached $90 \pm 2\%$. Mean grain
259   sizes varied across the sites, with the innermost site (core 1058MUC) showing the largest
260   grain sizes, ranging from 8.8 μm to 13.3 μm. The middle site (core 1161MUC) exhibited
261   a slightly smaller range, from 7.9 μm to 13.0 μm, while the outermost site (core
262   1159MUC) ranged from 8.3 μm to 11.0 μm.

263   Mineral-specific surface area (SA) values decreased with distance from the inner
264   fjord site. Core 1058MUC showed values between 10.0 m²/g and 16.5 m²/g, core
265   1161MUC ranged from 8.6 m²/g to 13.9 m²/g, and core 1159MUC exhibited the lowest
266   range, from 8.3 m²/g to 11.0 m²/g.

267

4.2 ^{210}Pb geochronology

269   The depth profiles of total ^{210}Pb (^{210}Pb$_{tot}$) and excess ^{210}Pb (^{210}Pb$_{ex}$) activities for the
270   two cores are displayed in Fig. 3. A sediment core collected in 2000 by Zaborska et al.
271   (2006) from inner Kongsfjorden, near the core 1058MUC site, showed a sedimentation
272   rate (SR) of ~0.15 cm/yr based on ^{210}Pb dating. However, core 1058MUC was excluded
273   from ^{210}Pb analysis due to the potential for high sedimentation rates and intense sediment
274   mixing near glacier fronts, which can disrupt sediment stratigraphy and reduce the

reliability of age-depth models (e.g., López et al., 2020; Schirone et al., 2022). Core 1161MUC exhibited $^{210}Pb_{tot}$ values ranging from 89.3 mBq/g to 233.0 mBq/g, while core 1159MUC showed a broader range from 22.1 mBq/g to 246.6 mBq/g. For $^{210}Pb_{ex}$, core 1161MUC had values between 59.6 mBq/g and 207.2 mBq/g, while core 1159MUC displayed a range from 9.3 mBq/g to 216.0 mBq/g. Based on these profiles, the sedimentation rate (SR) was calculated as 0.36 cm/yr at the middle site (core 1161MUC) and 0.12 cm/yr at the outermost site (core 1159MUC).

4.3 Bulk elemental and carbon isotopic compositions

The depth profiles of bulk elemental and carbon isotope parameters for the three sediment cores are shown in Fig. 4. The TOC content showed clear trends depending on the core location. Core 1058MUC had values ranging from 0.2 to 0.4 wt.% (average 0.3 $\pm$ 0.0 wt.%), while core 1161MUC ranged from 0.9 to 1.5 wt.% (average 1.2 $\pm$ 0.1 wt.%), and core 1159MUC exhibited the highest values, ranging from 1.9 to 2.5 wt.% (average 2.2 $\pm$ 0.2 wt.%). A similar pattern was observed for total nitrogen (N_{tot}) content: core 1058MUC ranged from 0.01 to 0.05 wt.%, core 1161MUC ranged from 0.08 to 0.13 wt.%, and core 1159MUC exhibited values from 0.22 to 0.26 wt.%. Previous studies conducted in various Svalbard fjords showed that surface sediments contained a substantial proportion of inorganic nitrogen, up to 70% of the N_{tot} content (Fig. S1A), with a significant correlation between inorganic nitrogen and clay mineral content (Schubert and Calvert, 2001; Winkelmann and Knies, 2005; Knies et al., 2007; Knies and Martinez, 2009; Kumar et al., 2016; Kim et al., 2023). Consistent with the strong linear relationship ($R^2 = 0.89$, Fig. S1A) between N_{tot} and organic nitrogen (N_{org}) reported in surface sediments from multiple Svalbard fjords (Kim et al., 2023), our subdataset from Kongsfjorden and Krossfjorden showed an even stronger correlation ($R^2 = 0.96$, Fig. S1B). This high degree of correlation allowed us to estimate N_{org} from N_{tot} using the derived regression equation: $N_{org} = 0.7863 \times N_{tot} - 0.0096$. Based on this method, the estimated N_{org} content ranged from 0.01 to 0.03 wt.% (average 0.01 $\pm$ 0.00 wt.%) for core 1058MUC, from 0.05 to 0.09 wt.% (average 0.07 $\pm$ 0.01 wt.%) for core 1161MUC, and from 0.14 to 0.17 wt.% (average 0.15 $\pm$ 0.01 wt.%) for core 1159MUC. However, it is important to consider that inorganic nitrogen content can vary with sediment type and depth, which may influence the accuracy of the estimated N_{org}. Therefore, although this regression-based method provided a practical approximation, caution was warranted

when interpreting the estimated N_{org} values, particularly in sediments with heterogeneous stratigraphy or mineral composition.

The molar N_{tot}/TOC ratios were lowest in core 1058MUC, varying from 0.04 to 0.12 (average 0.06 ± 0.02), followed by core1161MUC, ranging from 0.06 to 0.11 (average 0.07 ± 0.01), and core 1159MUC with values between 0.08 and 0.11 (average 0.09 ± 0.01). The N_{org}/TOC ratios showed a similar pattern, being lower than the corresponding N_{tot}/TOC ratios, with core 1058MUC ranging from 0.03 to 0.08, core 1161MUC ranging from 0.04 to 0.07, and core1159MUC ranging from 0.05 to 0.07.

The $\delta^{13}C_{org}$ values exhibited a distinct offshore-increasing trend. Core 1058MUC displayed values ranging from –24.6 ‰ to –22.5 ‰ (average -23.5 ± 0.5 ‰). Core 1161MUC values ranged from –23.9 ‰ to –22.3 ‰ (average -23.2 ± 0.3 ‰), while core 1159MUC showed the most enriched values, ranging from –23.5‰ to –22.4 ‰ (average -22.7 ± 0.3 ‰). A similar pattern was observed for $\Delta^{14}C_{org}$ values, which increased from the innermost to the outermost site. Core 1058MUC ranged from –839.2 ‰ to –743.5 ‰ (average -793.9 ± 31.1 ‰). Core 1161MUC exhibited values from –555.9 ‰ to –405.7 ‰ (average -504.9 ± 44.0 ‰), and core 1159MUC showed values between –469.3 ‰ and –396.7 ‰ (average -433.5 ± 21.7 ‰).

4.4 Lignin phenol compositions

The depth profiles of the products of alkaline CuO oxidation for the three sediment cores are presented in Fig. 5. Total lignin phenol concentrations, which represent the sum of eight lignin-derived monomeric phenols (vanillyl (V), syringyl (S), and cinnamyl (C) units), normalized to TOC, showed clear variation with depth and location. Core 1058MUC had the highest total lignin phenol concentrations, ranging from 0.24 to 0.66 mg/gOC (average 0.40 ± 0.12 mg/gOC). Cores 1161MUC and 1159MUC showed similar concentrations, with overlapping ranges and comparable average values. Specifically, core 1161MUC ranged from 0.07 to 0.19 mg/gOC (average 0.14 ± 0.04 mg/gOC), and core 1159MUC ranged from 0.06 to 0.22 mg/gOC (average 0.12 ± 0.04 mg/gOC), indicating no significant difference between the two sites.

The S/V and C/V ratios, which reflect the type of organic material derived from vascular plants, followed a consistent pattern, with higher values at the innermost site. For core 1058MUC, the S/V ratio ranged from 0.01 to 0.63, and the C/V ratio ranged from 0.00 to 0.55. At the middle site (core 1161MUC), the S/V ratio ranged from 0.07 to

341   0.36, and the C/V ratio from 0.00 to 0.25, both decreasing relative to the inner site. Core

342   1159MUC showed S/V values between 0.13 and 0.49 and C/V values from 0.14 to 0.41,

343   which were higher than those at the middle site but still lower than those at the innermost

344   site.

345   The 3,5-Bd/V ratios, indicative of the extent of lignin degradation, varied

346   significantly among the sites. Core 1058MUC showed values from 0.06 to 0.55, while

347   core 1161MUC exhibited a broader range from 0.47 to 2.59. Core 1159MUC had the

348   highest 3,5-Bd/V ratios, ranging from 0.59 to 2.46, indicating more extensive oxidation

349   of lignin-derived compounds at the outer site. Similarly, the (Ad/Al)v ratios, which

350   represent the degree of oxidative alteration of lignin side chains, exhibited a comparable

351   trend. Core 1058MUC showed values between 0.22 and 0.89, while core 1161MUC

352   ranged from 0.40 to 1.60. The highest values were observed in core 1159MUC, ranging

353   from 0.37 to 1.74, further supporting the trend of increased lignin degradation in

354   sediments toward the outer fjord.

355

356 **5. Discussion**

357 **5.1 Grain size end-member modelling**

358   Grain-size end-member (EM) modeling identifies representative patterns within a

359   sediment's grain-size distribution, allowing for inferences about the influence of

360   depositional processes based on variations in the relative abundances of each EM (van

361   Hateren et al., 2018). Following the approach used by Ahn et al. (2024) in Wijdefjorden,

362   northern Svalbard, grain-size EM modeling was performed to analyze variations in the

363   grain-size distribution of the three cores investigated in this study. Two candidate Q

364   values were identified (Fig. S2), with R^2 values exceeding 0.6 for each core (Fig. S3).

365   The optimal Q value was selected by comparing the extracted EMs with the analyzed

366   grain-size distribution curves (Fig. S4). From the three cores, a total of eight EMs were

367   extracted (Fig. S5) and subsequently classified into four primary EM groups (Fig. 6A).

368   EM1 primarily consisted of fine-grained sediment (very fine to medium silt, 2–16 μm),

369   with EM1b having a relatively coarser-dominant mode (primary mode: 9.3–15.5 μm, very

370   fine to medium silt: 54.3–59.7%) compared to EM1a (primary mode: 8.2–9.3 μm, very

371   fine to medium silt: 62.2–66.8%). In contrast, EM2 was dominated by coarser grains

372   (medium to very coarse silt, 8–63 μm, 66.4%), with a coarse primary mode of 29.3 μm.

373   Notably, EM3 exhibited a wide range of grain sizes, including both fine and coarse

374   particles, with modes at 9.3 and 81.2 μm.

375   The EM results revealed that EM1a and EM1b, primarily consisting of the finest

376   grains, were present in all three sediment cores (Fig. 6B). These fine-grained sediments

377   are generally deposited through size-dependent settling of suspended particles from

378   meltwater and/or glaciofluvial discharge (Ó Cofaigh and Dowdeswell, 2001; Forwick and

379   Vorren, 2009; Elverhøi et al., 1980). The flocculation in seawater further promotes their

380   settling (Meslard et al., 2018), facilitating the transport of both EM1a and EM1b from the

381   inner to the outer fjord. The distinction between EM1a and EM1b deposition is influenced

382   by the strength of meltwater discharge, with stronger discharge suspending and

383   transporting relatively coarser particles found in EM1b (Ahn et al., 2024). In contrast,

384   coarse-grained sediments, primarily represented by EM2, were observed only at the

385   innermost site (core 1058MUC), situated closest to the glacier front (Fig. 6B). This area

386   is likely influenced by bottom currents driven by subglacial meltwater outflow (Meslard

387   et al., 2018; Torsvik et al., 2019). The scarcity of fine particles in EM2 reflects the

388   winnowing effect of these currents, which preferentially remove finer material and leave

389   behind coarser sediments (Vorren et al., 1984). Such glacially influenced environments

390   are typically characterized by poorly sorted sediments (Hass, 2002), and strong bottom

391   currents (Ahn et al., 2024) that promote coarse-grained deposition near glacier fronts. On

392   the other hand, EM3 contains both fine and coarse particles, with a coarse mode reaching

393   81.2 μm, significantly larger than the principal mode of EM2. EM3 was found exclusively

394   in the middle core (1161MUC), located at the central site of Kongsfjorden. This

395   distribution corresponds to the presence of multiple sediment sources in the mid-fjord

396   region, where fluvial inputs from land-terminating glaciers, such as the Bayelva River

397   near Ny-Ålesund, deliver mixed sediments and terrestrial OC (D'Angelo et al., 2018;

398   Husum et al., 2019).

399

400   **5.2 Source of sedimentary organic carbon: bulk parameters**

401   The TOC values of the three sediment cores varied significantly along

402   Kongsfjorden, with the innermost core (1058MUC) having the lowest TOC (average 0.3

403   ± 0.0 wt.%), and the outermost core (1159MUC) the highest (average 2.2 ± 0.2 wt.%)

404   (Fig. 4). This variation was also reflected in the TOC/SA ratio (Figs. 7A-7B), which

405   indicates OC loading and serves as a measure of OC preservation efficiency (Keil et al.,

406   1994; Mayer et al., 1994; Stein et al., 2004; Zonneveld et al., 1997). Values between 0.4

and 1.0 suggest a balance between OC supply and degradation (Keil et al., 1997). However, values below 0.4 are observed in the innermost core. In Kongsfjorden, D'Angelo et al. (2018) reported that lithogenic material accounted for the dominant sediment fraction (64–78%), and Svendsen et al. (2002) highlighted significant deposition of mineral material in the inner fjord. Therefore, the lower OC loading in the innermost core (1058MUC) is likely attributed to the deposition of coarse-grained terrestrial minerals (see Fig. 6B) that dilute the OC content. In contrast, higher OC loading in the middle and outer cores, with values greater than 1.0, suggests enhanced OC preservation efficiency, likely due to adsorption onto fine-grained minerals (see Fig. 6B) that reduce degradation (Keil et al., 1994; Mayer, 1994; Blair and Aller, 2012).

Similar to TOC, both N_{tot} and N_{org} values were highest in the outermost core (1159MUC) compared to the middle (1161MUC) and innermost (1058MUC) cores (Fig. 7C; see also Fig. 4). TOC and N (both N_{tot} and N_{org}) contents in all three cores largely overlapped with those reported for surface sediments from Kongsfjorden and Krossfjorden (Kim et al., 2023 and references therein). In contrast, small drifted ice samples containing ice-rafted debris (IRD) from the fjords had lower TOC (0.1 ± 0.0 wt.%) and N_{tot} (0.04 ± 0.01 wt.%) contents, whereas coal samples from Kongsfjorden exhibited significantly higher values (TOC: 50.8 ± 11.1 wt.%; N_{tot}: 0.86 ± 0.04 wt.%). The N_{tot}/TOC and N_{org}/TOC ratios were also highest in the outermost core (Fig. 7D; see also Fig. 4). Additionally, the $\delta^{13}C_{org}$ values were more enriched in the outermost core (Fig. 7D; see also Fig. 4), suggesting an increased contribution of marine OC to sedimentary OC toward the outer fjord. Notably, the $\delta^{13}C_{org}$ values from all three cores fell within the range observed in the small drifted ice containing IRD samples (–21.8 ± 2.1 ‰), coal samples (–24.4 ± 1.6 ‰), and surface sediments from Kongsfjorden (–23.0 ± 0.7 ‰). However, the $\delta^{13}C_{org}$ values of most surface sediments and small drifted ice containing IRD samples from Krossfjorden were higher than those from Kongsfjorden, generally falling outside the range observed in all three cores. This difference may be associated with the Quaternary marine deposits exposed in Krossfjorden (Fig. S6, Dallmann and Elvevold, 2015), which could supply older, ^{13}C-enriched marine-derived OC. These observations suggest that the contribution of Krossfjorden to sedimentary OC in all three cores was minimal. The $\Delta^{14}C_{org}$ values of the innermost core (1058MUC) were more depleted than those of the other two cores (Figs. 7E-7F). Similarly, small drifted ice containing IRD and surface sediment samples collected near the marine-terminating glacier front in Kongsfjorden exhibited similarly depleted values. Notably, the $\Delta^{14}C_{org}$

values of the other two cores fell between those of the glacier-front samples and those from the outer fjord. These results align with Kim et al. (2023), who suggested that the significant depletion of $\Delta^{14}C_{org}$ in the surface sediments of Svalbard fjords indicates that recently fixed terrestrial and marine OC alone cannot account for the sedimentary OC. Instead, a substantial amount of old OC, likely from petrogenic and soil-derived sources, contributes to the sedimentary OC in Kongsfjorden.

The relationship between TOC and mean grain size showed no clear correlation, with the sediments predominantly consisting of silt fractions (Fig. S7A). Similarly, TOC content did not exhibit a distinct relationship with sediment sorting values (Fig. S7B). The sediments were generally poorly sorted, with high silt content, a characteristic feature of glacial environments, where deposits are typically incompletely sorted due to the non-selective nature of glacial transport (Singh et al., 2019). The consistently poor sorting observed across all morphological zones, along with the absence of correlation between TOC and mean grain size, suggests a glacier-fed depositional system influenced by variable hydrodynamic conditions driven by meltwater discharge. At the middle site, the presence of EM3 indicates a contribution of terrestrial material via fluvial processes. However, the proportion of EM3 was relatively low (18.2 ± 14.9%) compared to EM1a and EM1b (81.8 ± 14.9%; Fig. 6), suggesting that glacial meltwater remains the dominant sediment delivery mechanism at this site, with only a minor influence from surface runoff processes. Overall, the sedimentary characteristics of Kongsfjorden indicate a fjord environment significantly influenced by glacial input. The repeated cycles of glacial advance and retreat have resulted in the accumulation of sediments with varied grain sizes and sorting patterns, reflecting the dynamic and complex interplay between terrestrial and marine OC processes within this glaciated fjord system.

5.3 Source of sedimentary organic carbon: lignin phenol parameters

In a previous study conducted in Svalbard fjords, Kim et al. (2023) defined two OC components (petrogenic OC and biogenic OC) to identify the source of ^{14}C-depleted OC in sedimentary OC. To further investigate the contributions of biogenic OC sources to Kongsfjorden, we analyzed lignin phenols obtained through alkaline CuO oxidation. Lignin phenols serve as valuable terrestrial biomarkers because they are exclusively synthesized by terrestrial higher plants (Hedges and Mann, 1979; Goñi et al., 2005). The ratios of S/V and C/V are used to evaluate the relative contributions of four components:

non-woody angiosperms, woody angiosperms, non-woody gymnosperms, and woody gymnosperms (Hedges and Mann, 1979; Goñi and Hedges, 1995). In the three Kongsfjorden cores, lignin phenols primarily consisted of a mixture of non-woody gymnosperm OC with inputs from gymnosperm wood-derived tissues, along with some contributions from non-woody angiosperms, consistent with previous studies (Fig. 8A). The strong gymnosperm signal observed in both surface and downcore sediments, despite the current dominance of angiosperm vegetation in the Svalbard archipelago, suggests a substantial contribution of OC from older terrestrial sources, such as permafrost-stored material. This implies that the terrestrial OC preserved in these sediments likely reflects inputs from past vegetation communities, rather than representing solely contemporary plant cover. Lignin phenol concentrations were highest in the innermost core (1058MUC) compared to the other two cores (Fig. 8B; see also Fig. 5), and fell within the range observed in surface sediments from Svalbard fjords, including Kongsfjorden and Krossfjorden (Figs. S8A and S9A).

3,5-Bd is primarily produced during soil degradation processes, leading to its enrichment in soils (e.g., Prahl et al., 1994; Goñi et al., 2000; Houel et al., 2006; Otto and Simpson, 2006). As a result, the 3,5-Bd/V ratio is widely used to assess the extent of lignin degradation and to trace inputs of soil-derived OC to aquatic systems (e.g., Prahl et al., 1994; Goñi et al., 2000; Houel et al., 2006; Otto and Simpson, 2006). Similarly, the (Ad/Al)v ratio reflects lignin oxidation, as the conversion of aldehyde functional groups into acidic phenols through propyl side-chain modification serves as a key indicator of lignin degradation in sedimentary organic matter (e.g., Hedges and Ertel, 1982; Goñi and Hedges, 1992; Otto and Simpson, 2006). (Ad/Al)v ratios below 0.3 typically indicate relatively fresh vascular plant detritus, whereas values exceeding 0.5 are generally associated with extensively altered soils with significantly depleted ^{14}C signatures (e.g., Hedges and Ertel, 1982; Goñi and Hedges, 1992; Otto and Simpson, 2006). Among the three cores, both 3,5-Bd/V and (Ad/Al)v ratios were lowest in the innermost core (1058MUC) (Figs. 8C and 8D; see also Fig. 5). Notably, coal samples also exhibited relatively low values, averaging 0.48 for the 3,5-Bd/V ratio and 0.49 for the (Ad/Al)v ratio, similar to those of the innermost core (1058MUC). Both the 3,5-Bd/V and (Ad/Al)v ratios were higher in the outermost core (1159MUC) compared to the middle (1161MUC) and innermost (1058MUC) cores, indicating a higher degree of lignin degradation toward the outer fjord. This trend likely reflects cumulative degradation processes occurring during offshore transport rather than differences in terrestrial OC sources alone. Notably,

508   the inter-site variation was more pronounced for the 3,5-Bd/V ratio than for the (Ad/Al)v
509   ratio.

510   Previously, Kim et al. (2023) suggested that biogenic OC includes not only recently
511   fixed terrestrial and marine biomass but also pre-aged OC from soils, which can be
512   transported to fjords through glacial erosion and surface runoff. Therefore, we examined
513   the lignin phenol concentrations and (Ad/Al)v ratios of these biogenic OC sources—
514   plant-derived, soil-derived, and marine OC (Fig. S8). Most core sediments exhibited
515   lower lignin phenol concentrations and (Ad/Al)v ratios compared to the average values
516   of soils collected in the Ny-Ålesund and Longyearbyen regions. Thus, the soil values
517   encompass the range observed in all three cores and most surface sediments collected in
518   Svalbard fjords. However, surface sediments from Krossfjorden exhibited distinct
519   (Ad/Al)v ratios and $\delta^{13}C_{org}$ values, which fell outside the soil range. This difference may
520   result from the complex bedrock types present in Svalbard fjords (Fig. S6), which can
521   influence OC characteristics (Kim et al., 2023). These findings suggest that the
522   contribution of Krossfjorden to the sedimentary OC in all three cores was limited.

523

524   **5.4 Four OC source apportionments**

525   In this study, we adopted the OC source classification concept from the surface
526   sediment study in Svalbard fjords (Kim et al., 2023) and defined four distinct sedimentary
527   OC sources: petrogenic, soil-derived, plant-derived, and marine OC. To estimate the
528   relative proportions of these OC sources, we applied a four-source apportionment
529   approach based on $\Delta^{14}C_{org}$, $\delta^{13}C_{org}$, and lignin parameters such as the (Ad/Al)v ratio and
530   lignin phenol concentrations, using a Monte Carlo (MC) analysis. End-member values
531   for each OC source, as reported in Kim et al. (2023; Table S1), were used in the analysis.

532   Firstly, similar to the previous study by Kim et al. (2023), the relative proportions
533   of the four OC sources were calculated using Method 1, based on $\Delta^{14}C_{org}$, $\delta^{13}C_{org}$, and the
534   (Ad/Al)v ratio (Fig. 9). The petrogenic OC fraction was highest in core 1058MUC,
535   located at the innermost site, with an average of 79.2 ± 3.4%. This was followed by core
536   1161MUC (average 44.7 ± 5.7%) and core 1159MUC (average 37.8 ± 5.0%). In contrast,
537   marine OC fractions were highest in core 1159MUC at the outermost site (average 44.0
538   ± 5.2%), followed by core 1161MUC (average 38.4 ± 7.8%) and core 1058MUC (average
539   19.0 ± 3.9%).

540   Secondly, we calculated the relative proportions of the four OC sources using
541   Method 2, which is based on $\Delta^{14}C_{org}$, $\delta^{13}C_{org}$, and lignin phenol concentrations. This

17

method was chosen because previous studies used lignin phenol concentrations for source mixing models, assuming a value of 0 for marine phytoplankton (Tesi et al., 2016; Pempkowiak et al., 2020). To validate this approach, we first applied Method 2 to surface sediments previously investigated by Kim et al. (2023). Overall, the estimated relative contributions of the four OC sources were within a similar range to those reported in the earlier study, and the spatial distribution pattern exhibited similar trends between both approaches (Fig. S10). For the three sediment cores in this study, the results from Method 2 were also consistent with those from Method 1. Petrogenic OC fractions were highest in core 1058MUC, located at the innermost site (average $79.2 \pm 3.3\%$), followed by cores 1161MUC (average $46.6 \pm 4.4\%$) and 1159MUC (average $40.7 \pm 1.7\%$) (Fig. 9). In contrast, marine OC fractions were greatest in core 1159MUC at the outermost site (average $50.4 \pm 4.7\%$), followed by core 1161MUC (average $42.9 \pm 5.2\%$) and core 1058MUC (average $16.5 \pm 3.2\%$). These findings suggest that Method 2 did not significantly alter the trends observed from Method 1. However, it is important to note that some surface sediments from Kongsfjorden and Krossfjorden exhibited (Ad/Al)v ratios outside the range of soil values (Fig. S9B). In contrast, the lignin phenol concentration data were well within the expected range for soils (Fig. S9A). Given this, Method 2 appears to be a more appropriate approach than Method 1 for assessing the relative proportions of the four OC sources in the Svalbard fjords.

Nonetheless, both methods showed that the plant-derived OC fraction contributed minimally compared to dominant sources such as petrogenic and marine OC. However, soil-derived OC contributions were higher in the middle (1161MUC) and outer (1159MUC) cores than in the innermost core (1058MUC), suggesting an additional input likely associated with surface runoff. This is supported by the presence of EM3 in core 1161MUC (Fig. 6B), indicative of significant input of both fine and coarse particles, a feature not observed in the other two cores. Given that core 1161MUC is situated closer to the Byelva River (Fig. 1), the occurrence of EM3 at this site likely reflects the localized influence of surface runoff. This runoff facilitates the transport of terrestrial material, especially soil-derived OC, into the fjord via riverine discharge from the adjacent catchment. This mechanism is consistent with previous studies, which have shown that surface runoff significantly influences the biogeochemical composition of particulate and dissolved matter in Kongsfjorden (e.g., Hop et al., 2002; Svendsen et al., 2002). These inputs are known to deliver high loads of suspended sediments, nutrients, and terrigenous OC, especially during the melt season when hydrological connectivity between the land

576   and fjord is enhanced. The proximity of core 1161MUC to the Byelva River mouth

577   therefore increases its susceptibility to these runoff-derived materials, which can be

578   subsequently advected toward the outer fjord.

579

580   **5.5 Potential future implications on carbon dynamics**

581   The bulk OC AR was 0.47 ± 0.06 g/cm²/yr at the middle site (core 1161MUC),

582   higher than the outermost site (core 1159MUC), which had a value of 0.26 ± 0.03 g/cm²/yr

583   (data not shown). The ARs of the four OC sources, determined by both Methods 1 and 2,

584   are presented in Fig. 10. For core 1161MUC, petrogenic OC ARs were similar between

585   Method 1 (0.18 ± 0.03 g/cm²/yr) and Method 2 (0.18 ± 0.02 g/cm²/yr). Among biogenic

586   sources, marine OC had the highest ARs (0.15 ± 0.03 g/cm²/yr for Method 1; 0.17 ± 0.03

587   g/cm²/yr for Method 2), two to four times higher than soil-derived OC and 20–70 times

588   higher than plant-derived OC. Similarly, for core 1159MUC, petrogenic OC ARs were

589   consistent across both methods (0.05 ± 0.01 g/cm²/yr), with marine OC showing the

590   highest biogenic ARs (0.05 ± 0.01 g/cm²/yr for Method 1; 0.06 ± 0.01 g/cm²/yr for

591   Method 2), exceeding those of soil-derived and plant-derived OC.

592   For all petrogenic and biogenic OC sources, ARs were higher at the middle site

593   (core 1161MUC) than at the outermost site (core 1159MUC) (Fig. 10). This spatial

594   difference likely reflects the middle site's closer proximity to glacial and fluvial sediment

595   inputs, including the tidewater glaciers (e.g., Kronebreen and Kongsbreen) and the

596   Bayelva River near Ny-Ålesund. Its location may have facilitated more efficient delivery

597   and deposition of sediments and associated OC, resulting in higher ARs. Notably, marine

598   OC ARs at core 1161MUC showed an increasing trend since approximately the 1970s,

599   while petrogenic OC ARs decreased over the same period. In contrast, no clear temporal

600   trends were observed in either petrogenic or marine OC ARs at the outermost site (Fig.

601   S11). This increase in marine OC ARs at the middle site (Fig. 11A) coincides with a shift

602   in sediment composition, characterized by increasing relative abundances of EM1b (Fig.

603   11B), suggesting intensified meltwater discharge from marine-terminating glaciers. This

604   discharge was likely driven by increased AW inflow, which enhanced basal melting of

605   tidewater glaciers. Being situated closer to these glaciers, the middle site appears more

606   sensitive to variability in AW inflow. Since increased AW inflow to fjords reduces sea

607   ice cover and delivers nutrients that enhance marine productivity, this process supports

608   greater marine OC burial. In contrast, the outermost site, under more stable AW influence,

609   exhibited relatively consistent marine OC burial over time. Additionally, its lower SRs, a

consequence of its greater distance from the glacier front, may obscure short-term variations in OC deposition. Overall, the differing trends in marine OC ARs between the middle and outermost sites likely reflect differences in hydrographic and sedimentary dynamics, with the middle site more responsive to glacial and oceanographic variability associated with AW inflow.

The rise in marine OC ARs coincides with broader climatic and environmental changes in the Svalbard region. Since the 1970s, surface air temperatures in Ny-Ålesund have increased at a rate four times faster than the global average from 1975 to 2014 (Fig. 11C, Wei et al., 2016). Concurrently, the Barents Sea summer sea ice extent has declined rapidly (Fig. 11D, NSIDC; National Snow and Ice Data Center, http://nsidc.org/data/seaice_index), and the Blomstrandbreen glacier has experienced significant retreat (Fig. 11D, Burton et al., 2016). These changes suggest a strong link between climate warming and shifts in Kongsfjorden's carbon dynamics. Notably, during the same period, integrated temperatures (50 to 300 m water depth) from the transect across 78°N, in the core of the WSC in western Svalbard, also showed an increasing trend (Fig. 11C, Tesi et al., 2021). This suggests a connection between the observed warming of AW and broader regional climatic and environmental changes. Longer-term environmental reconstructions support this connection, with studies reporting increased AW inflow and associated productivity in Kongsfjorden in the early 20th century (Husum et al., 2019; Tesi et al., 2021). Ingrosso et al. (2025) also documented rapid greening of western Svalbard during the same period, which they attributed to extremely low sea ice extent, driven primarily by the strong advection of warm AW into Arctic fjords. This historical context highlights the likely influence of enhanced AW inflow on the rise in marine OC ARs recorded at the middle site (core 1161MUC) since the 1970s, with increased marine productivity and OC burial contributing to this rise while driving the concurrent decline in petrogenic OC ARs.

6. Conclusions

In this study, we investigated three multicores collected from Kongsfjorden, Svalbard, to explore the spatial and temporal dynamics of sedimentary OC over recent centuries. Bulk parameter analyses indicate that Kongsfjorden was the primary source of OC in the sediments, with minor contributions from Krossfjorden. Additionally, a substantial amount of old OC, likely derived from petrogenic and soil sources, was present in the sedimentary OC in Kongsfjorden. To estimate the relative proportions of

644 OC sources, we applied a four-source apportionment approach based on $\Delta^{14}C_{org}$, $\delta^{13}C_{org}$,

645 and lignin parameters, including the (Ad/Al)v ratio and lignin phenol concentrations,

646 using MC analysis. Our results revealed that petrogenic OC fractions were highest at the

647 innermost site, while marine OC fractions dominated at the outermost site. The plant-

648 derived OC fraction contributed minimally compared to petrogenic and marine OC, while

649 soil-derived OC was more substantial at the middle and outermost sites, suggesting

650 enhanced input from surface runoff. For all OC sources, ARs were higher at the middle

651 site than at the outermost site. Notably, marine OC ARs at the middle site showed an

652 increasing trend since approximately the 1970s, likely reflecting enhanced AW inflow,

653 which boosted marine productivity and OC burial. These findings underscore the

654 significant role of AW inflow in reshaping carbon dynamics in Svalbard fjords over the

655 past few decades, highlighting the sensitivity of Arctic fjords to climate shifts. More

656 importantly, our study suggests that the marked increase in AW inflow to Kongsfjorden

657 during the 20th century likely occurred in two distinct phases, around the early 1900s and

658 the 1970s. This pattern reflects a two-step process driven by complex and not yet fully

659 understood mechanisms. To better constrain the timing, drivers, and consequences of AW

660 variability, we emphasize the need for future research that integrates high-resolution

661 climate modeling with sediment core records from Svalbard. Such an integrated approach

662 will be essential for improving projections of climate and carbon cycle feedbacks in the

663 rapidly warming Arctic. Given their role as critical OC reservoirs, Arctic fjords may

664 function as both sources and sinks of carbon in a warming climate, emphasizing the need

665 for further research to assess the long-term consequences of climate-induced changes on

666 regional carbon cycling.

667

668 **Data availability**

669   All the primary data related to this article are available online at Korea Polar Data

670 Center (http://dx.doi.org/doi:10.22663/KOPRI-KPDC-00002831) or upon request to the

671 corresponding author (Jung-Hyun Kim, jhkim123@kopri.re.kr).

672

673 **Supplement**

674   The supplementary material related to this article is published together with the

675 article.

676

677 **Author contributions**

678   D.K. and J.-H.K. designed the study, interpreted the majority of the data, and wrote
679   the manuscript. Y.K.A., M.F., and S.I.N. contributed to sample acquisition. D.K.
680   conducted the biomarker analyses, while Y.K.A. performed the grain size analyses and
681   the end-member modeling. All authors commented on the manuscript and contributed to
682   its revision.
683

699   **References**
700   Ahn, Y., Joe, Y. J., Jang, K., Kim, J.-H., Son, Y. J., Forwick, M., Hong, S., Nam, S.-I.:
701   Post-glaciation depositional changes in Wijdefjorden, northern Svalbard, using
702   grain-size end-member modelling. Mar. Geol., 472, 107306,
703   https://doi.org/10.1016/j.margeo.2024.107306, 2024.
704   Appleby, P. G.: Dating recent sediments by 210 Pb: problems and solutions. Seminar on
705   Dating of sediments and determination of sedimentation rate, pp p. 7–24,
706   https://inis.iaea.org/records/vtsmx-fvz88, 1998.
707   Appleby, P. G., Oldfield, F.: The calculation of lead-210 dates assuming a constant rate
708   of supply of unsupported ^{210}Pb to the sediment. Catena, 5, 1–8,
709   https://doi.org/10.1016/S0341-8162(78)80002-2, 1978.

Årthun, M., Eldevik, T., Smedsrud, L., Skagseth, O., Ingvaldsen, R.: Quantifying the influence of Atlantic heat on Barents Sea ice variability and retreat, J. Clim., 25, 4736–4743, http://doi.org/10.1175/JCLI-D-11-00466.1, 2012.

Bianchi, T. S., Cui, X., Blair, N. E., Burdige, D. J., Eglinton, T. I., Galy, V.: Centers of organic carbon burial and oxidation at the land-ocean interface, Org. Geochem., 115, 138–155, https://doi.org/10.1016/j.orggeochem.2017.09.008, 2017.

Bianchi, T. S., Cui, X., Blair, N. E.: Fjords as aquatic critical zones (ACZs), Earth Sci. Rev., 203, 103145, https://doi.org/10.1016/j.earscirev.2020.103145, 2020.

Blair, N. E., and Aller, R. C.: The fate of terrestrial organic carbon in the marine environment. Annu. Rev. Mar. Sci., 4, 401–423, https://doi.org/10.1146/annurev-marine-120709-142717, 2012.

Brogi, S. R., Jung, J. Y., Ha, S.-Y., and Hur, J.: Seasonal differences in dissolved organic matter properties and sources in an Arctic fjord: Implications for future conditions, Sci. Total Environ., 694, 133740, https://doi.org/10.1016/j.scitotenv.2019.133740, 2019.

Burton, D. J., Dowdeswell, J. A., Hogan, K. A., Noormets, R.: Marginal fluctuations of a Svalbard surge-type tidewater glacier, Blomstrandbreen, since the Little Ice Age: A record of three surges, Arctic, Antarctic, and Alpine Research, 48, 411–426, http://doi.org/10.1657/AAAR0014-094, 2016.

Cantoni, C., Hopwood, M. J.,Clarke, J. S., Chiggiato, J.,Achterberg, E. P., Cozzi, S.: Glacial drivers of marinebiogeochemistry indicate a future shiftto more corrosive conditions in anArctic fjord, J. Geophys. Res. Biogeosci., 125, e2020JG005633, https://doi.org/10.1029/2020JG005633, 2020.

Choudhary, S., Neelavanan, K., Saalim, S. M.: Microplastics in the surface sediments of Krossfjord-Kongsfjord system, Svalbard, Arctic, Mar. Pollut. Bull., 176, 113452, http://doi.org/10.1016/j.marpolbul.2022.113452, 2022.

Cottier, F. R., Nilsen, F., Inall, M. E., Gerland, S., Tverberg, V., Svendsen, H.: Wintertime warming of an Arctic shelf in response to large-scale atmospheric circulation, Geophys. Res. Lett., 34, L10607, http://doi.org/10.1029/2007GL029948, 2007.

D'Angelo, A., Giglio, F., Miserocchi, S., Sanchez-Vidal, A., Aliani, S., Tesi, T.: Multi-year particle fluxes in Kongsfjorden, Svalbard, Biogeosciences, 15, 5343–5363, https://doi.org/10.5194/bg-15-5343-2018, 2018.

742   Dahlke, F. T., Wohlrab, S., Butzin, M., Pörtner, H.-O.: Thermal bottlenecks in the life

743   cycle define climate vulnerability of fish, Sciences, 369, 65–70,

744   http://doi.org/10.1126/science.aaz3658, 2020.

745   Dallmann, W. K., Elvevold, S.: Bedrock geology. Geoscience Atlas of Svalbard, Re-port

746   Series 148, Norsk Polarinstitutt, Tromsø, pp.133–173,

747   http://hdl.handle.net/11250/2580810, 2015.

748   De Rovere, F., Langone, L., Schroeder, K., Miserocchi, S., Giglio, F., Aliani, S., and

749   Chiggiato, J.: Water masses variability in inner Kongsfjorden (Svalbard) during

750   2010–2020, Front. Mar. Sci., 9, 741075,

751   https://doi.org/10.3389/fmars.2022.741075, 2022.

752   Elverhøi, A., Liestøl, O. and Nagy, J.: Glacial erosion, sedimentation and microfauna in

753   the inner part of Kongsfjorden, Spitsbergen, Norsk Polarinstitutt Skrifter, 172, 33–

754   58, http://core.ac.uk/reader/30910780#page=35, 1980.

755   Forwick, M., Vorren, T. O.: Late Weichselian and Holocene sedimentary environments

756   and ice rafting in Isfjorden, Spitsbergen, Palaeogeogr. Palaeoclimatol. Palaeoecol.,

757   280, 258–274, http://doi.org/10.1016/j.palaeo.2009.06.026, 2009.

758   Friedlingstein, P., et al.: Global carbon budget 2020, Earth Syst. Sci. Data, 12, 3269–3340,

759   http://doi.org/10.5194/essd-12-3269-2020, 2020.

760   Gealy, E. L.: Saturated bulk density, grain density, and porosity of sediment cores from

761   the western equatorial Pacific: Leg 7, Glomar Challenger. Initial Reports of the

762   Deep Sea Drilling Project, 7, 1081–1104, 1971.

763   Goñi, M. A., and Hedges, J. I.: Lignin dimers: structures, distribution, and potential

764   geochemical applications, Geochim. Cosmochim. Acta, 56, 4025–4043,

765   https://doi.org/10.1016/0016-7037(92)90014-A, 1992.

766   Goñi, M. A., and Hedges, J. I.: Sources and reactivities of marine-derived organic matter

767   in coastal sediments as determined by alkaline CuO oxidation, Geochim.

768   Cosmochim. Acta, 59, 2965–2981, https://doi.org/10.1016/0016-7037(95)00188-3,

769   1995.

770   Goñi, M. A., Yunker, M. B., MacDonald, R. W., and Eglinton, T. I.: Distribution and

771   sources of organic biomarkers in arctic sediments from the Mackenzie River and

772   Beaufort Shelf, Mar. Chem., 71, 23–51, https://doi.org/10.1016/S0304-

773   4203(00)00037-2, 2000.

774   Goñi, M. A., Yunker, M. B., MacDonald, R. W., and Eglinton, T. I.: The supply and

775   preservation of ancient and modern components of organic carbon in the Canadian

Beaufort Shelf of the Arctic Ocean, Mar. Chem., 93, 53–73, https://doi.org/10.1016/j.marchem.2004.08.001, 2005.

Hamilton, E. L.1971 Elastic properties of marine sediments, J. Geophys. Res., 76, 293–635, https://doi.org/10.1190/1.1440168, 1971.

Hass, H. C.: A method to reduce the influence of ice-rafted debris on a grain size record from northern Fram Strait, Arctic Ocean, Polar Res., 21, 299–306, http://doi.org/10.1111/j.1751-8369.2002.tb00084.x, 2002.

Hedges, J. I., and Ertel, J. R.: Characterization of lignin by gas capillary chromatography of cupric oxide oxidation products, Anal. Chem., 54, 174–178, https://doi.org/10.1021/ac00239a007, 1982.

Hedges, J. I., and Mann, D. C.: The characterization of plant tissues by their lignin oxidation products, Geochim. Cosmochim. Acta, 43, 1803–1807, https://doi.org/10.1016/0016-7037(79)90028-0, 1979.

Hop, H., et al.: The marine ecosystem of Kongsfjorden, Svalbard, Polar Res., 21, pp.167-208, http://doi.org/10.1007/978-3-319-46425-1_1, 2002.

Houel, S., Louchouarn, P., Lucotte, M., Canuel, R., and Ghaleb, B.: Translocation of soil organic matter following reservoir impoundment in boreal systems: Implications for in situ productivity, Limnol. Oceanogra., 51, 1497–1513, https://doi.org/10.4319/lo.2006.51.3.1497, 2006.

Husum, K., et al.: The marine sedimentary environments of Kongsfjorden, Svalbard: An archive of polar environmental change, Polar Res., 38, 3380, https://doi.org/10.33265/polar.v38.3380, 2019.

Ingrosso, G., Ceccarelli, C., Giglio, F., Giordano, P., Hefter, J., Langone, L., Miserocchi, S., Mollenhauer, G., Nogarotto, A., Sabino, M., Tesi, T.: Greening of Svalbard in the twentieth century driven by sea ice loss and glaciers retreat, Commun. Earth Environ., 6, 30, http://doi.org/10.1038/s43247-025-01994-y, 2025.

Ito, H., and S. Kudoh,: Characteristics of water in Kongsfjorden, Svalbard, Proc. NIPR Symp. Polar Meteorol. Glaciol., 11, 211–232, 1997.

Jernas, P., et al.: Annual changes in Arctic fjord environment and modern benthic foraminiferal fauna: Evidence from Kongsfjorden, Svalbard, Global Planet. Change, 163, 119–140, 2018.

Jordà-Molina, È., Renaud, P. E., Silberberger, M. J., Sen, A., Bluhm, B. A., Carroll, M. L., Ambrose Jr., W. G., Cottier, F., Reiss, H.: Seafloor warm water temperature anomalies impact benthic macrofauna communities of a high-Arctic cold-water

fjord. Mar. Envrion. Res., 189. 106046, http://doi.org/10.1016/j.marenvres.2023.106046, 2023.

Keil, R. G., Tsamakis, E., Fuh, C. B., Giddings, J. C., Hedges, J. I.: Mineralogical and textural controls on the organic composition of coastal marine sediments: Hydrodynamic separation using SPLITT-fractionation, Geochim. Cosmochim. Acta, 58, 879–893, https://doi.org/10.1016/0016-7037(94)90512-6, 1994.

Keil, R. G., Mayer, L. M., Quay, P. D., Richey, J. E., Hedges, J. I.: Loss of organic matter from riverine particles in deltas, Geochim. Cosmochim. Acta, 61, 1507–1511, https://doi.org/10.1016/S0016-7037(97)00044-6, 1997.

Kim, J.-H., Peterse, F., Willmott, V., Klitgaard Kristensen, D., Baas, M., Schouten, S., Sinninghe Damsté, J.S.: Large ancient organic matter contributions to Arctic marine sediments (Svalbard), Limnol. Oceanogr., 56, 1463–1474, http://doi.org/10.4319/1o.2011.56.4.1463, 2011.

Kim, D., Kim, J.-H., Tesi, T., Kang, S., Nogarotto, A., Park, K., Lee, D.-H., Jin, Y.K., Shin, K.-H., Nam, S.-I.: Changes in the burial efficiency and composition of terrestrial organic carbon along the Mackenzie Trough in the Beaufort Sea, Estuar. Coastal Shelf Sci., 275, 107997, https://doi.org/10.1016/j.ecss.2022.107997, 2022.

Kim, D., Kim, J.-H., Ahn, Y., Jang, K., Jung, J. Y., Bae, M., Nam, S.-I.: Large contributions of petrogenic and aged soil-derived organic carbon to Arctic fjord sediments in Svalbard, Sci. Rep., 13, 17935, https://doi.org/10.1038/s41598-023-45141-z, 2023.

Knies, J., Martinez, P.: Organic matter sedimentation in the western Barents Sea region: Terrestrial and marine contribution based on isotopic composition and organic nitrogen content. Nor. J. Geol., 89, 79–89, 2009.

Knies, J., Brookes, S., Schubert, C. J.: Re-assessing the nitrogen signal in continental margin sediments: New insights from the high northern latitudes, Earth Planet. Sci. Lett., 253, 471–484, http://doi.org/10.1016/j.epsl.2006.11.008, 2007.

Krajewska, M., Szymczak-Zyla, M., Tylmann, W., Kowalewska, G.: Climate change impact on primary production and phytoplankton taxonomy in Western Spitsbergen fjords based on pigments in sediments, Global Planet. Change, 189, 103158, http://doi.org/10.1016/j.gloplacha.2020.103158, 2020.

Kumar, V., Tiwari, M., Nagoji, S., Tripathi, S.: Evidence of anomalously low $\delta^{13}C$ of marine organic matter in an Arctic Fjord, Sci. Rep., 6, 36192, http://10.1038/srep36192, 2016.

844 Lind, S., Ingvaldsen, R. B., Furevik, T.: Arctic warming hotspot in the northern Barents
845   Sea linked to declining sea-ice import, Nat. Clim. Change, 8, 634–639, 2018.

846 Mayer, L. M.: Surface area control of organic carbon accumulation in continental shelf
847   sediments, Geochim. Cosmochim. Acta, 58, 1271–1284,
848   https://doi.org/10.1016/0016-7037(94)90381-6, 1994.

849 McGovern, M., Borgå, K., Heimstad, E., Ruus, A., Christensen, G., Evenset, A.: Small
850   Arctic rivers transport legacy contaminants from thawing catchments to coastal
851   areas in Kongsfjorden, Svalbard, Environ. Pollut., 304, 119191,
852   https://doi.org/10.1016/j.envpol.2022.119191, 2022.

853 Meslard, F., Bourrin, F., Many, G., Kerherve, P.: Suspended particle dynamics and fluxes
854   in an Arctic fjord (Kongsfjorden, Svalbard), Estuar. Coast. Shelf Sci., 204, 212–
855   224, http://doi.org/10.1016/j.ecss.2018.02.020, 2018.

856 Nam, S.-I.: Late Quaternary glacial history and paleoceanographic reconstructions along
857   the East Greenland continental marine: evidence from high-resolution records of
858   stable isotopes and ice-rafted debris, Rep. Polar Res., 241, pp. 21,
859   https://epic.awi.de/id/eprint/26419/1/BerPolarforsch1997241.pdf, 1997.

860 Nuth, C., Kohler, J., Konig, M., von Deschwanden, A., Hagen, J. O., Kaab, A., Moholdt,
861   G., Pettersson, R.: Decadal changes from a multi-temporal glacier inventory of
862   Svalbard. The Cryosphere, 7, 1603–1621, http://doi.org/10.5194/tc-7-1603-2013,
863   2013.

864 Ó Cofaigh, C., Dowdeswell, J. A.: Laminated sediments in glacimarine environments:
865   diagnostic criteria for their interpretation, Quat. Sci. Rev., 20, 1411–1436,
866   http://doi.org/10.1016/S0277-3791(00)00177-3, 2001.

867 Otto, A., and Simpson, M. J.: Evaluation of CuO oxidation parameters for determining
868   the source and stage of lignin degradation in soil, Biogeochem., 80, 121–142,
869   https://doi.org/10.1007/s10533-006-9014-x, 2006.

870 Pempkowiak, J.: Limitation of lignin derivatives as biomarkers of land derived organic
871   matter in the coastal marine sediments, Oceanologia, 62, 374–386,
872   http://doi.org/10.1016/j.oceano.2020.04.004, 2020.

873 Polyakov, I. V., Pnyushkov, A. V., Alkire, M. B., Ashik, I. M., Baumann, T. M., Carmack,
874   E. C., Goszczko, I., Guthrie, J., Ivanov, V. V., Kanzow, T., Krishfield, R., Kwok,
875   R., Sundfjord, A., Morison, J., Remember, R., Yulin, A.: Greater role for Atlantic
876   inflows on sea-ice loss in the Eurasian Basin of the Arctic Ocean, Science, 356,
877   285–291, 2017.

878 Prahl, F. G., Ertel, J. R., Goñi, M. A., Sparrow, M. A., Eversmeyer, B.: Terrestrial organic
879   carbon contributions to sediments on the Washington margin, Geochim.
880   Cosmochim. Acta, 58, 3035–3048, https://doi.org/10.1016/0016-7037(94)90177-5,
881   1994.

882 Pramanik, A., Kohler, J., Lindback, K., How, P., Van Pelt, W., Liston, G., Schuler, T. V.:
883   Hydrology and runoff routing of glacierized drainage basins in the Kongsfjord area,
884   northwest Svalbard, The Cryosphere, http://doi.org/10.5174/tc-2020-197, 2020.

885 Rantanen, M., Karpechko, A. Y., Lipponen, A., Nordling, K., Hyvärinen, O., Ruosteenoja,
886   K., Räisänen, J.: The Arctic has warmed nearly four times faster than the globe
887   since 1979, Commun. Earth Environ., 3, 168, https://doi.org/10.1038/s43247-022-
888   00498-3, 2022.

889 Saloranta, T. M., Svendsen, H.: Across the Arctic front west of Spitsbergen: high-
890   resolution CTD sections from 1998–2000, Polar Research, 20, 177–184,
891   http://doi.org/10.3402/polar.v20i2.6515, 2001.

892 Schauer, U., Fahrbach, E., Osterhus, S., Rohardt, G.: Arctic warming through the Fram
893   Strait: Oceanic heat transport from 3 years of measurements, J. Geophys. Res.
894   Oceans, 109, C06026, https://doi.org/10.1029/2003JC001823, 2004.

895 Singh, D. S., Dubey, C. A., Kumar, D., Vishawakarma, B., Singh, A. K., Tripathi, A.,
896   Sharma, R.: Monsoon variability and major climatic events between 25 and 0.05 ka
897   BP using sedimentary parameters in the Gangotri glacier region, Garhwal Himalaya,
898   India. Quater. Inter., 507, 148–155, https://doi.org/10.1016/j.quaint.2019.06.024,
899   2019.

900 Skogseth, R., Asplin, L., Budgell, W. P., Eldevik, T., Gerland, S., Haugan, P., Zamelczyk,
901   K.: Variability and decadal trends in the Isfjorden (Svalbard) ocean climate and
902   circulation – An indicator for climate change in the European Arctic, Progr.
903   Oceanogr., 187, 102394, https://doi.org/10.1016/j.pocean.2020.102394, 2020.

904 Smith, R. W., Bianchi, T. S., Allison, M., Savage, C., Galy, V.: High rates of organic
905   carbon burial in fjord sediments globally, Nat. Geosci., 8, 450–453,
906   http://doi.org/10.1038/NGEO2421, 2015.

907 Stein, R., and MacDonald, R. W.: The organic carbon cycle in the Arctic Ocean, Springer.
908   https://doi.org/10.1007/978-3-642-18912-8, 2004.

909 Stuiver, M., and Polach, H. A.: Discussion: Reporting of 14C data. Radiocarbon, 19, 355–
910   363, https://doi.org/10.1017/S0033822200003672, 1977.

911 Svendsen, H., Beszczynska-Møller, A., Hagen, J. O., Lefauconnier, B., Tverberg, V.,
912   Gerland, S., Ørbæk, J. B.: The physical environment of Kongsfjorden–Krossfjorden,
913   an Arctic fjord system in Svalbard, Polar Res., 21, 133–166,
914   https://doi.org/10.3402/polar.v21i1.6479, 2002.

915 Tesi, T., Muschitiello, F., Smittenber, R. H., Jakobsson, M., Vonk, J. E., Hill, P.,
916   Andersson, A., Kirchner, N., Noormets, R., Dudarev, O., Semiletov, I., Gustafsson,
917   Ö.: Massive remobilization of permafrost carbon during past-glacial warming, Nat.
918   Commun., 7, 13653, http://doi.org/10.1038/ncomms13653, 2016.

919 Tesi, T., Muschitiello, F., Mollenhauer, G., Miserocchi, S., Langone, L., Ceccarelli, C.,
920   Panieri, G., Chiggiato, J., Nogarotto, A., Hefter, J., Ingrosso, G., Giglio, F.,
921   Giordano, P., Capotondi, L.: Rapid atlantification along the Fram Strait at the
922   beginning of the 20th century, Sci. Advances, 7, eabj2946,
923   http://doi.org/10.1126/sciadv.abj2946, 2021.

924 Torsvik, T., Albretsen, J., Sundfjord, A., Kohler, J., Sandvik, A. D., Skarohamar, J.,
925   Lindback, K., Everett, A.: Impact of tidewater glacier retreat on the fjord system:
926   Modeling present and future circulation in Kongsfjorden, Svalbard, Estuar. Coast.
927   Shelf Sci., 220, 152–165, http://doi.org/10.1016/j.ecss.2019.02.005, 2019.

928 Tverberg, V., Skogseth, R., Cottier, F., Sundfjord, A., Walczowski, W., Inall, M. E., Falck,
929   E., Pavlova, O., Nilsen, F.: The Kongsfjorden transect: seasonal and inter-annual
930   variability in hydrography, The Ecosystem of Kongsfjorden, Svalbard, 49–104,
931   http://doi.org/10.1007/978-3-319-46425-1_3, 2019.

932 van Hateren, J. A., Prins, M. A., van Balen, R. T.: On the genetically meaningful
933   decomposition of grain-size distributions: A comparison of different end-member
934   modelling algorithms, Sediment. Geol., 375, 49–71,
935   http://doi.org/10.1016/j.sedgeo.2017.12.003, 2018.

936 Vorren, T. O., Hald, M., Thomsen, E.: Quaternary sediments and environments on the
937   continental shelf off northern Norway, Mar. Geol., 57, 229–257,
938   http://doi.org/10.1016/0025-3227(84)90201-9, 1984.

939 Wei, T., Ding, M., Wu, B., Lu, C., and Wang, S.: Variations in temperature-related
940   extreme events (1975–2014) in Ny-Ålesund, Svalbard, Atmos. Sci. Lett., 17, 102–
941   108, https://doi.org/10.1002/asl.632, 2016.

942 Winkelmann, D., Knies, J.: Recent distribution and accumulation of organic carbon on
943   the continental marine west off Spitsbergen, Geochem. Geophys. Geosyst., 6,
944   Q09012, http://doi.org/10.1029.2005GC000916, 2005.

945 Zaborska, A., Pempkowiak, J., Papucci, C.: Some sediment characteristics and
946   sedimentation rates in an Arctic fjord (Kongsfjorden, Svalbard), Annu. Environ.
947   Prot., 8, pp.79–96, 2006.

948 Zhu, Z.-Y., Wu, Y., Liu, S.-M., Wenger, F., Hu, J., Zhang, J., Yao, P.: Organic carbon
949   flux and particulate organic matter composition in Arctic valley glaciers: Examples
950   from the Bayelva River and adjacent Kongsfjorden, Biogeosciences, 13, 975–987,
951   https://doi.org/10.5194/bg-13-975-2016, 2016.

952 Zonneveld, K. A. F., Versteegh, G. J. M., and de Lange, G. J.: Preservation of organic-
953   walled dinoflagellate cysts in different oxygen regimes: A 10,000 years natural
954   experiment. Mar. Micropaleontol., 29, 393–405, https://doi.org/10.1016/S0377-
955   8398(96)00032-1, 1997.

Figures

957

958

959

960
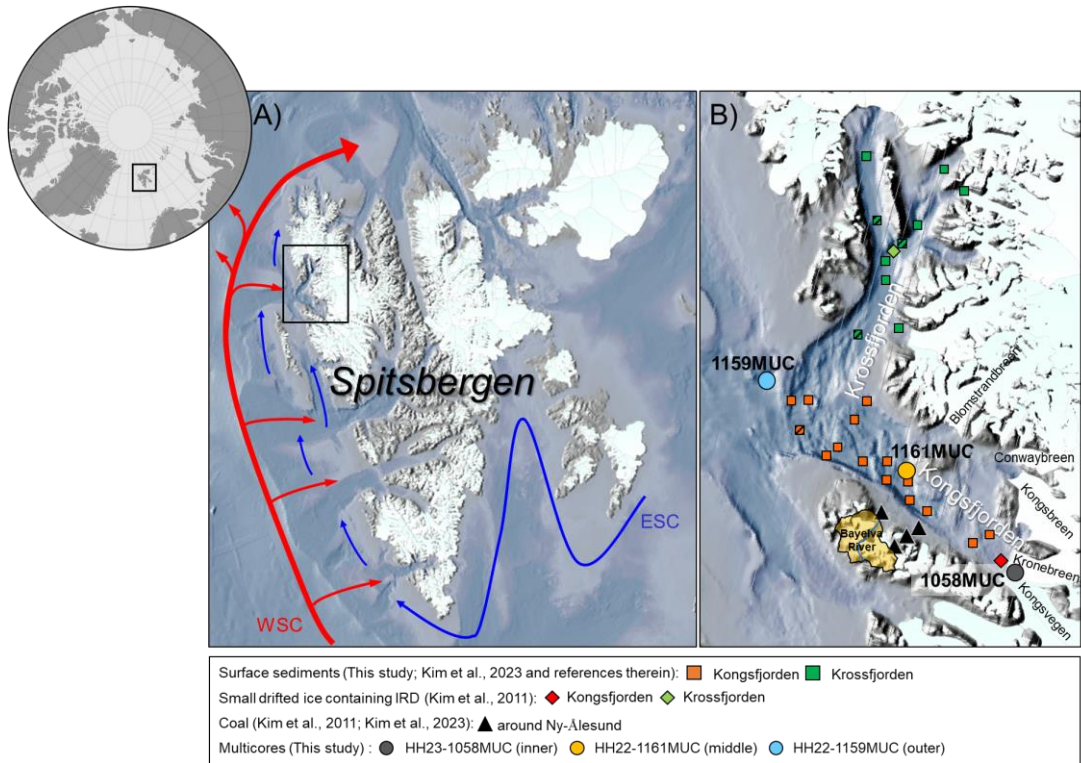
Fig. 1. Map of the study area showing (A) the Svalbard archipelago and (B) the sampling sites in Kongsfjoren and Krossfjorden considered in this study. White land areas indicate present-day glacier coverage. Red and blue arrows indicate the main Atlantic (West Spitsbergen Current, WSC) and Arctic (East Spitsbergen Current, ESC) water currents, respectively. Filled circles represent multicore sampling sites, while filled square, diamond, and triangle symbols indicate surface sediment, small drifted ice containing IRD, and coal sampling sites in Kongsfjorden and Krossfjorden. It should be noted that the surface sediment samples newly analyzed in this study are denoted by hashed square symbols. The map was generated using QGIS v3.14 (https://qgis.org/en/site/forusers/visualchangelog314/) based on IBCAOv4 (https://www.ngdc.noaa.gov/mgg/bathymetry/arctic/).

972
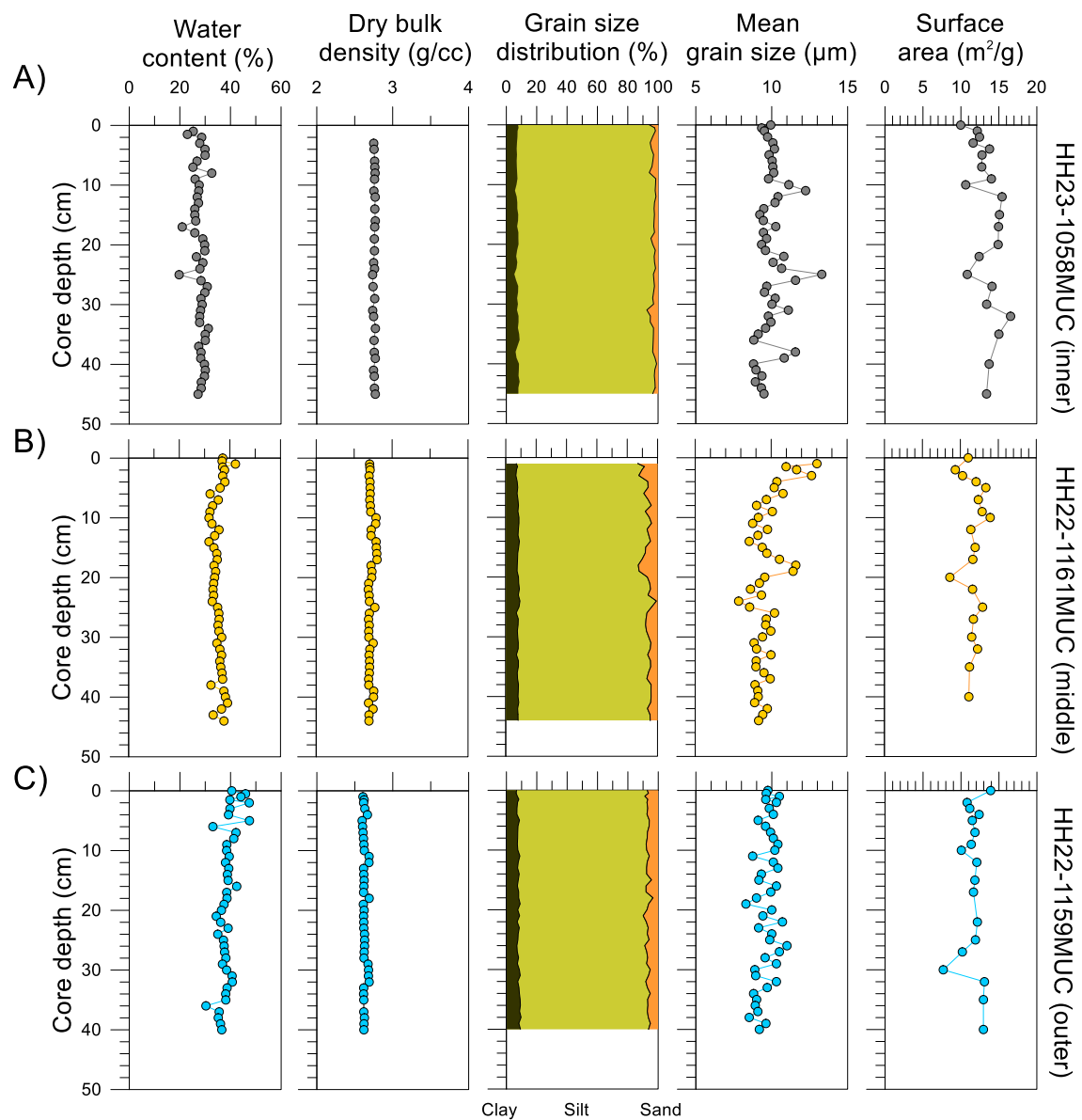
Fig. 2. Depth profiles of water content (%), dry bulk density (g/cc), grain size distribution (%), mean grain size (μm), and surface area (m²/g) for the cores (A) HH23-1058MUC, (B) HH22-1161MUC, and (C) HH22-1159MUC.
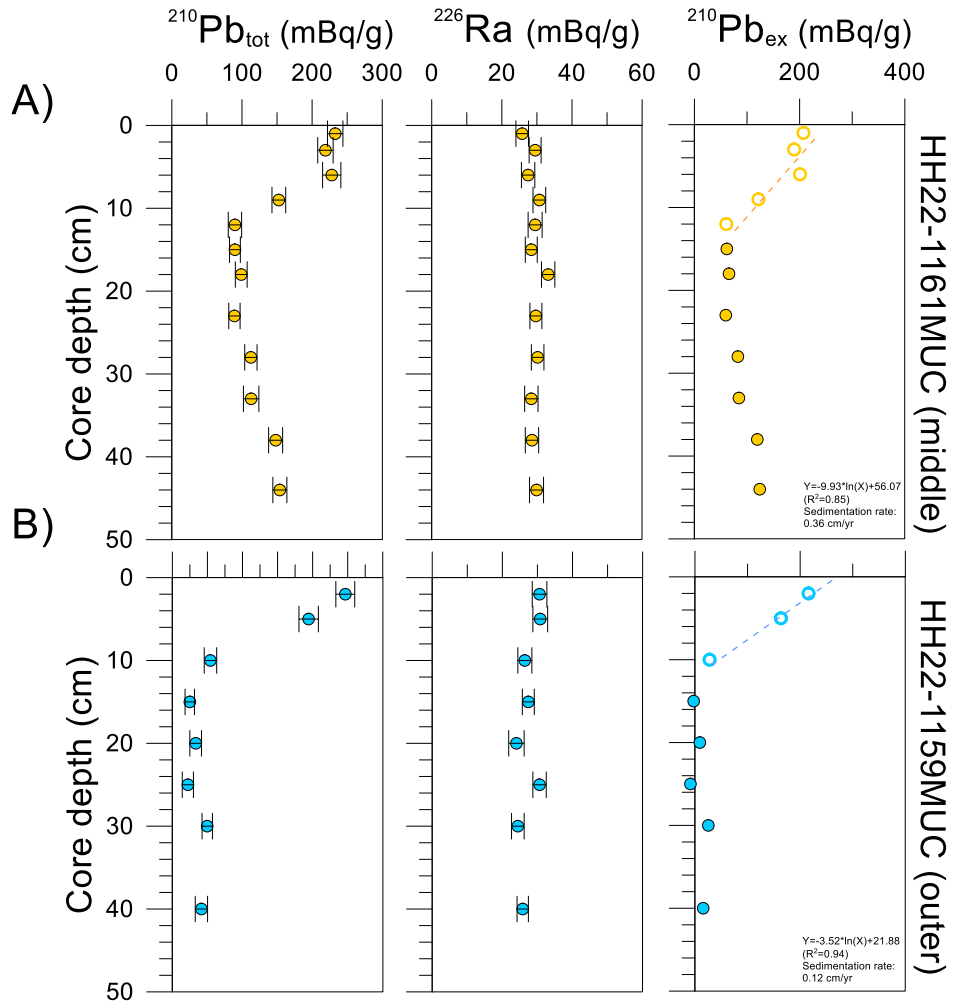
Fig. 3. Depth profiles of $^{210}Pb_{tot}$ (mBq/g), ^{226}Ra (mBq/g), and $^{210}Pb_{ex}$ (mBq/g) for the cores (A) HH22-1161MUC, and (B) HH22-1159MUC. Open circles indicate the data points used in the linear regressions (yellow and blue dotted lines) of the natural log-transformed $^{210}Pb_{ex}$ versus depth, which were applied to estimate sedimentation rates.

984
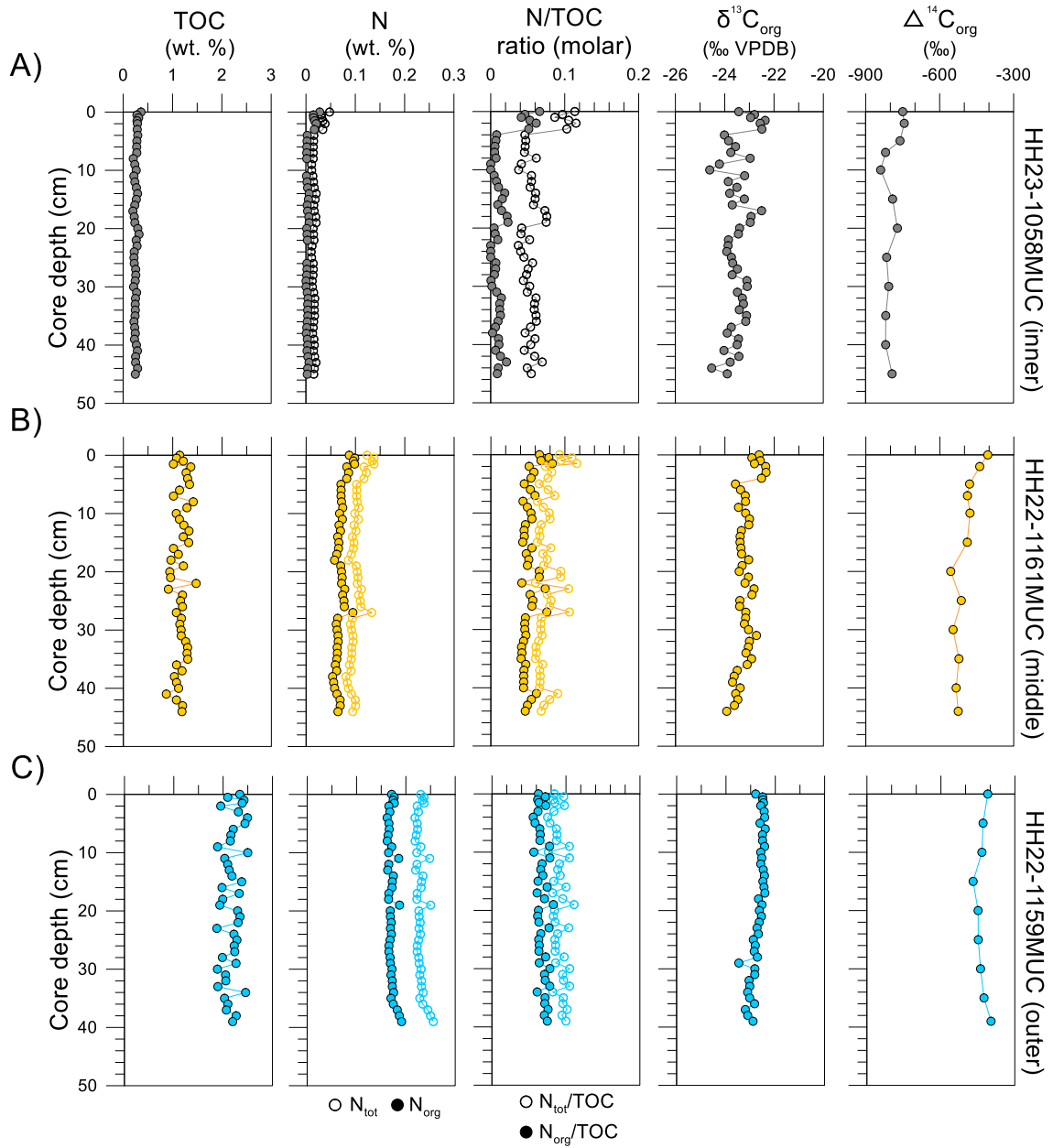
Fig. 4. Depth profiles of TOC (wt. %), N (wt. %), N/TOC ratios (molar), $\delta^{13}C_{org}$ (‰ VPDB), and $\Delta^{14}C_{org}$ (‰) for the cores (A) HH23-1058MUC, (B) HH22-1161MUC, and (C) HH22-1159MUC.

988
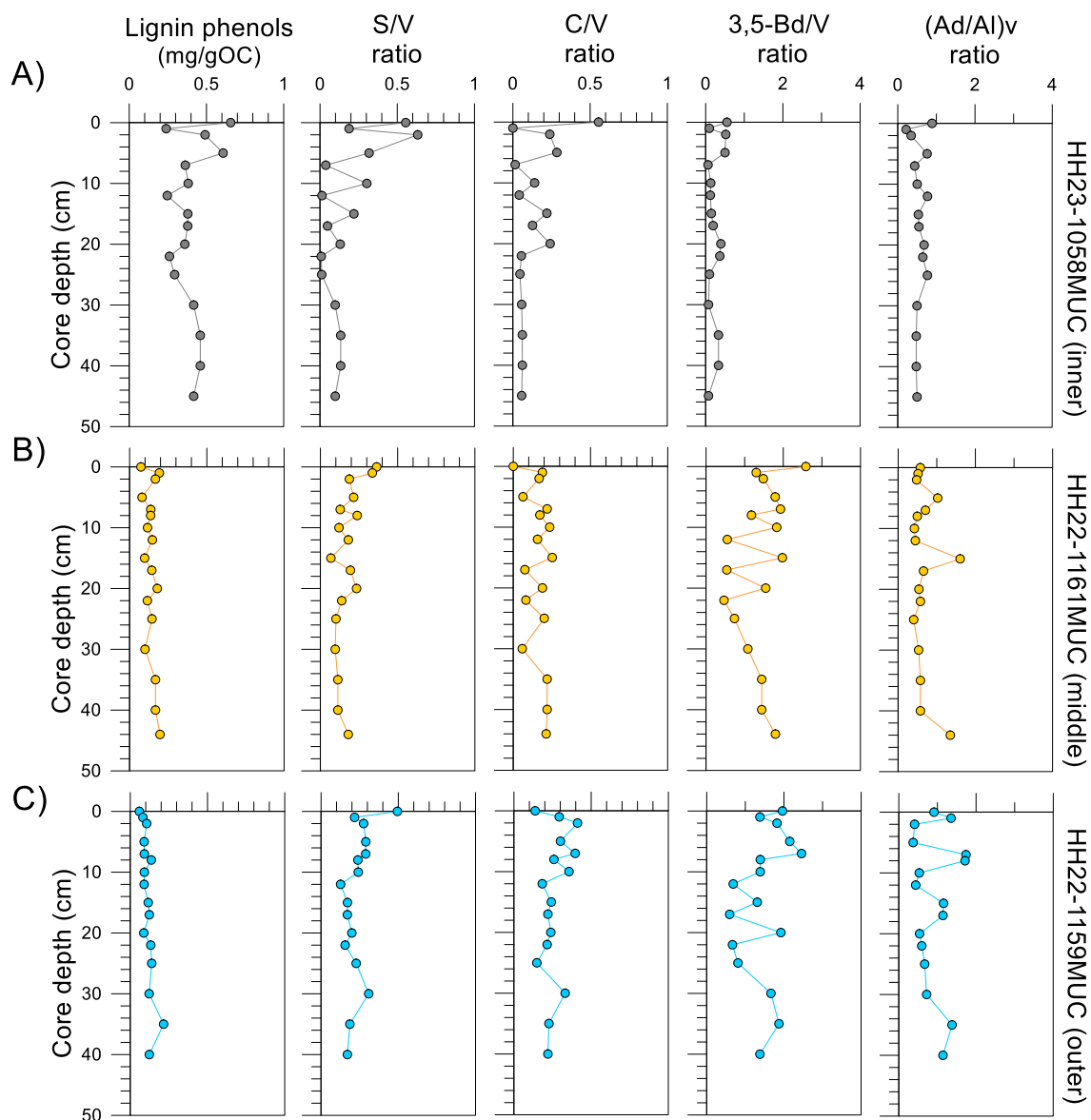
989   Fig. 5. Depth profiles of lignin phenol concentrations (mg/gOC), and S/V, C/V, 3,5-Bd/V,

990   and (Ad/Al)v ratios for the cores (A) HH23-1058MUC, (B) HH22-1161MUC, and (C)

991   HH22-1159MUC.

992
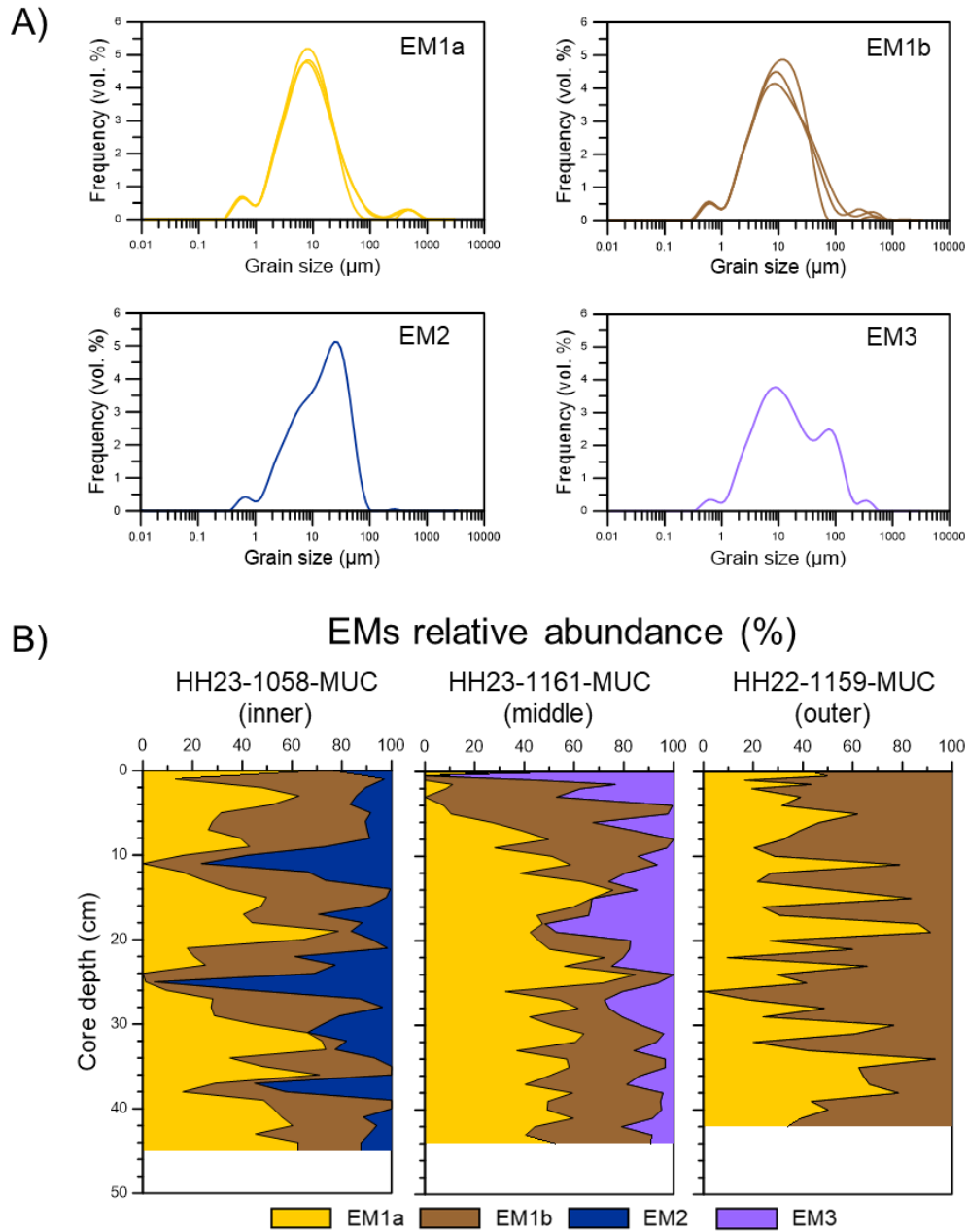
Fig. 6. (A) Classified grain-size end-member distribution curves from three cores, and (B) depth profiles showing the variation in the relative abundances of grain-size end-members (EM1a, EM1b, EM2, and EM3) in the three cores analyzed in this study.
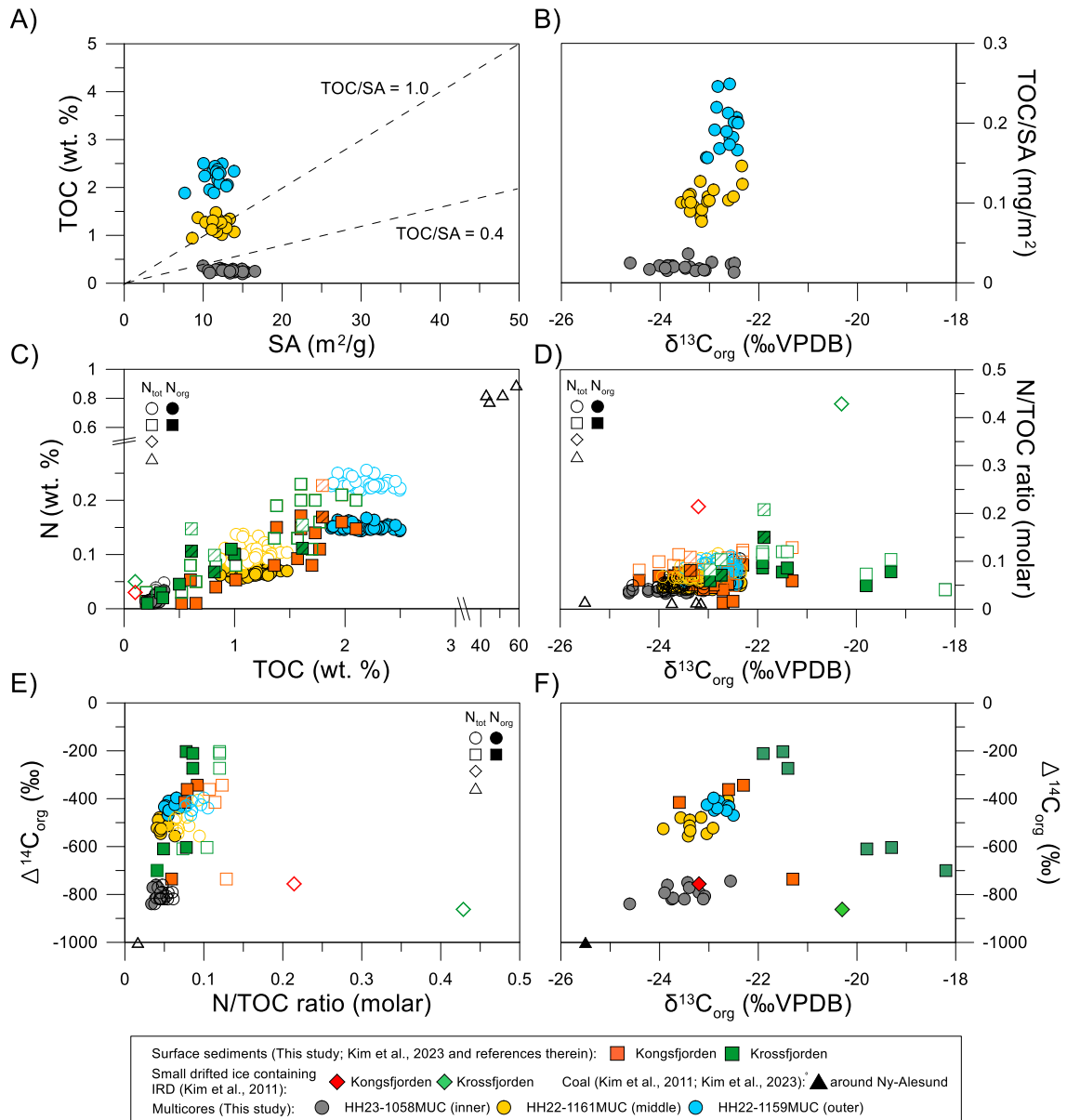
Fig. 7. Scatter plots of (A) SA (m²/g) versus TOC (wt.%), (B) $\delta^{13}C_{org}$ (‰ VPDB) versus TOC/SA (mg/m²), (C) TOC (wt.%) versus N_{tot} or N_{org} (wt.%), (D) $\delta^{13}C_{org}$ (‰ VPDB) versus N_{tot}/TOC (molar) ratios or N_{org}/TOC (molar) ratios, (E) N_{tot}/TOC (molar) ratios or N_{org}/TOC (molar) ratios versus $\Delta^{14}C_{org}$ (‰), and (F) $\delta^{13}C_{org}$ (‰ VPDB) versus $\Delta^{14}C_{org}$ (‰) for the three cores, compared with data from small drifted ice containing IRD (Kim et al., 2011), coals (Kim et al., 2011; Kim et al., 2023), and surface sediments (Kim et al., 2023 and this study). Note that the surface sediment samples newly analyzed in this study are denoted by hashed square symbols.

37
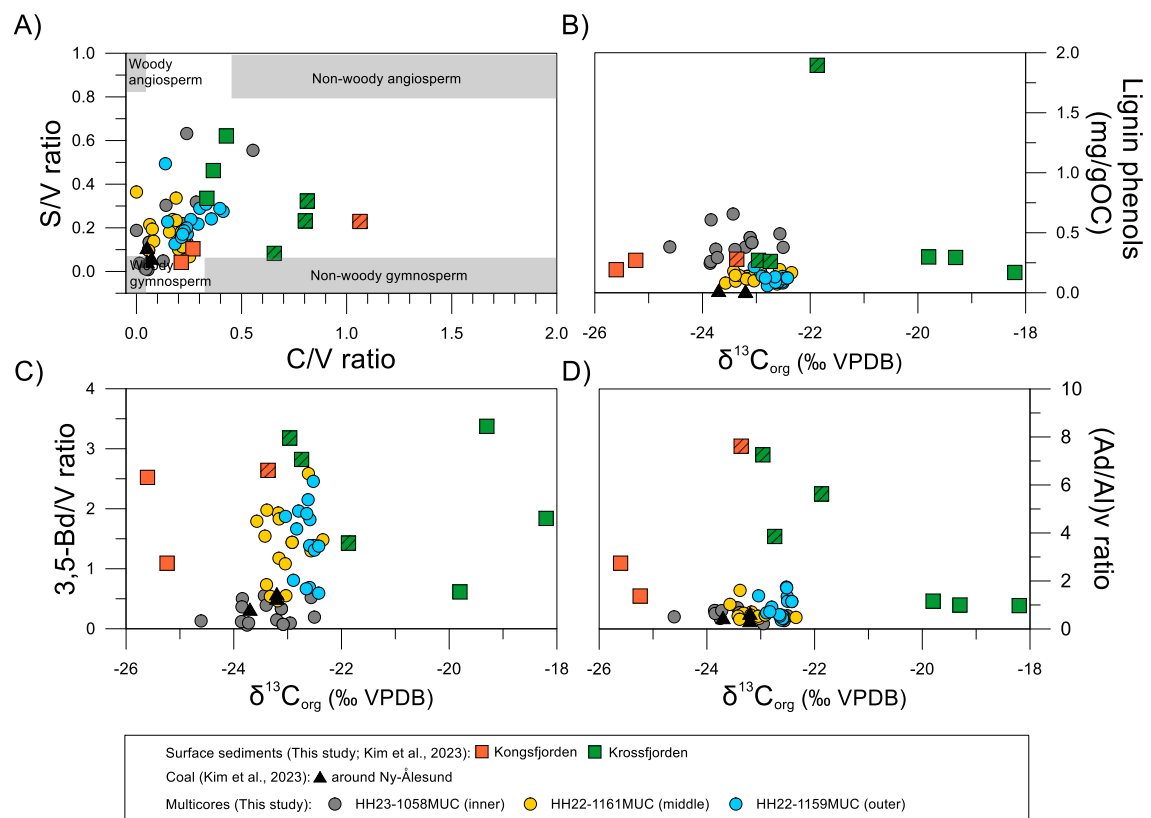
Fig. 8. Scatter plots of (A) C/V ratio versus S/V ratio, including the end-members for different vascular plant tissues (cf. Goñi et al., 2000), (B) $\delta^{13}C_{org}$ (‰ VPDB) versus lignin phenols (mg/gOC), (C) $\delta^{13}C_{org}$ (‰ VPDB) versus 3,5-Bd/V ratio, and (D) $\delta^{13}C_{org}$ (‰ VPDB) versus (Ad/Al)v ratio for the three cores, compared with data from coals (Kim et al., 2023) and surface sediments (Kim et al., 2023 and this study). Note that the surface sediment samples newly analyzed in this study are indicated by hashed square symbols.

1016
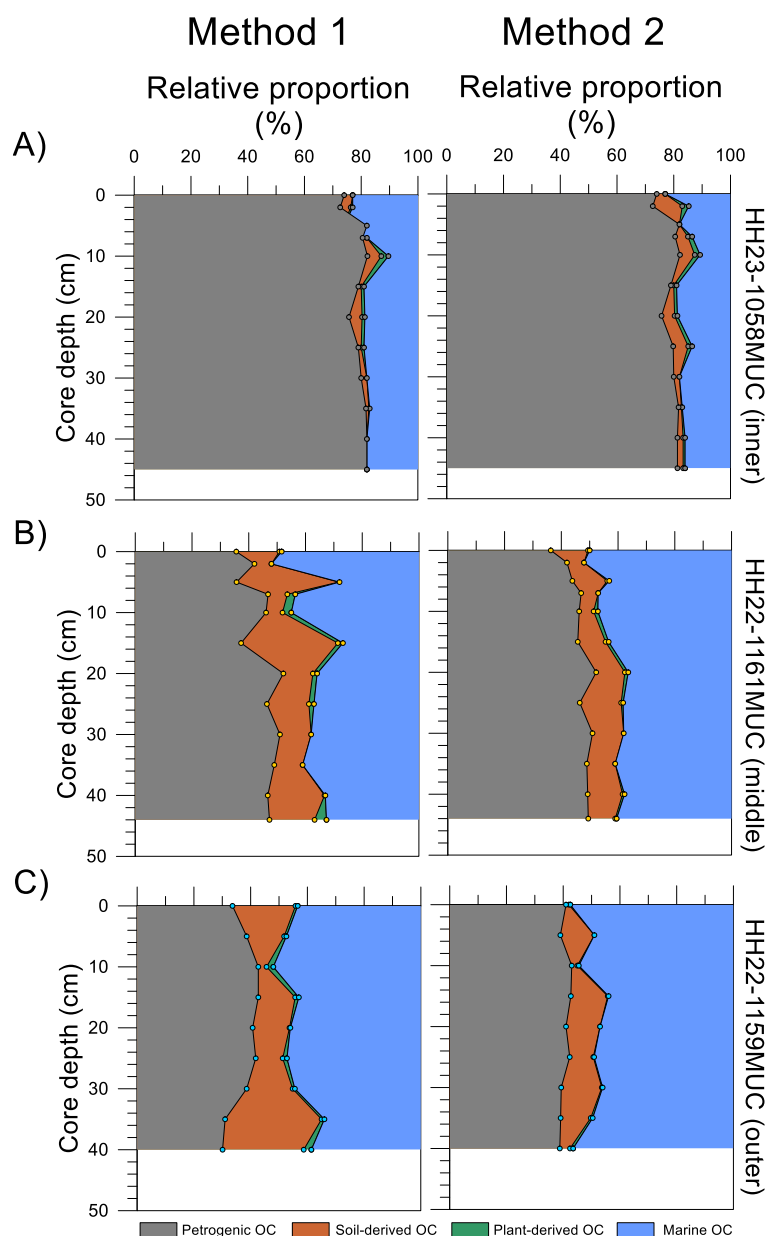
Fig. 9. Depth profiles showing the relative proportions of petrogenic, soil-derived, plant-derived, and marine OC, as determined using Method 1 (based on $\delta^{13}C_{org}$ (‰ VPDB), $\Delta^{14}C_{org}$ (‰), and (Ad/Al)v ratio) and Method 2 (based on $\delta^{13}C_{org}$ (‰ VPDB), $\Delta^{14}C_{org}$ (‰), and lignin phenols (mg/gOC)), for the cores (A) HH23-1058MUC, (B) HH22-1161MUC, and (C) HH22-1159MUC.
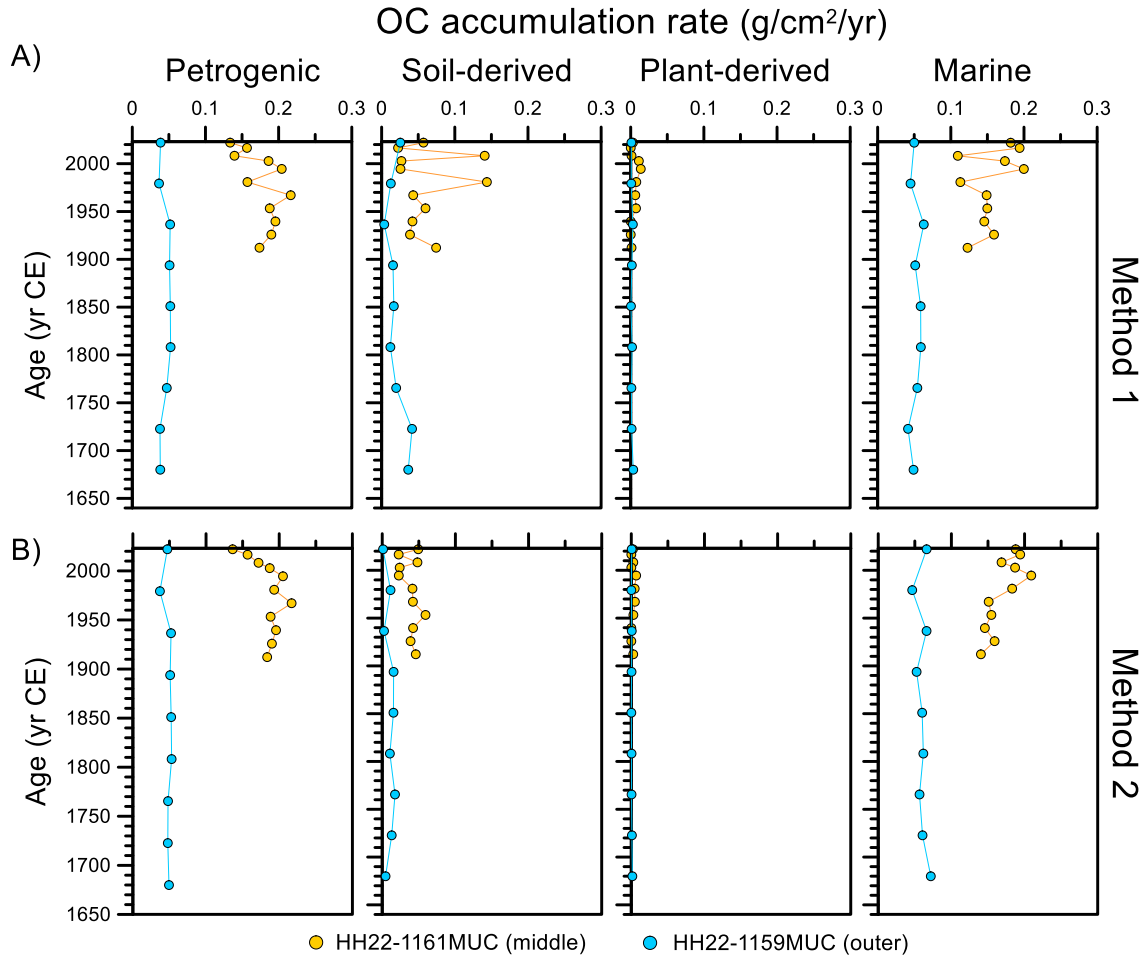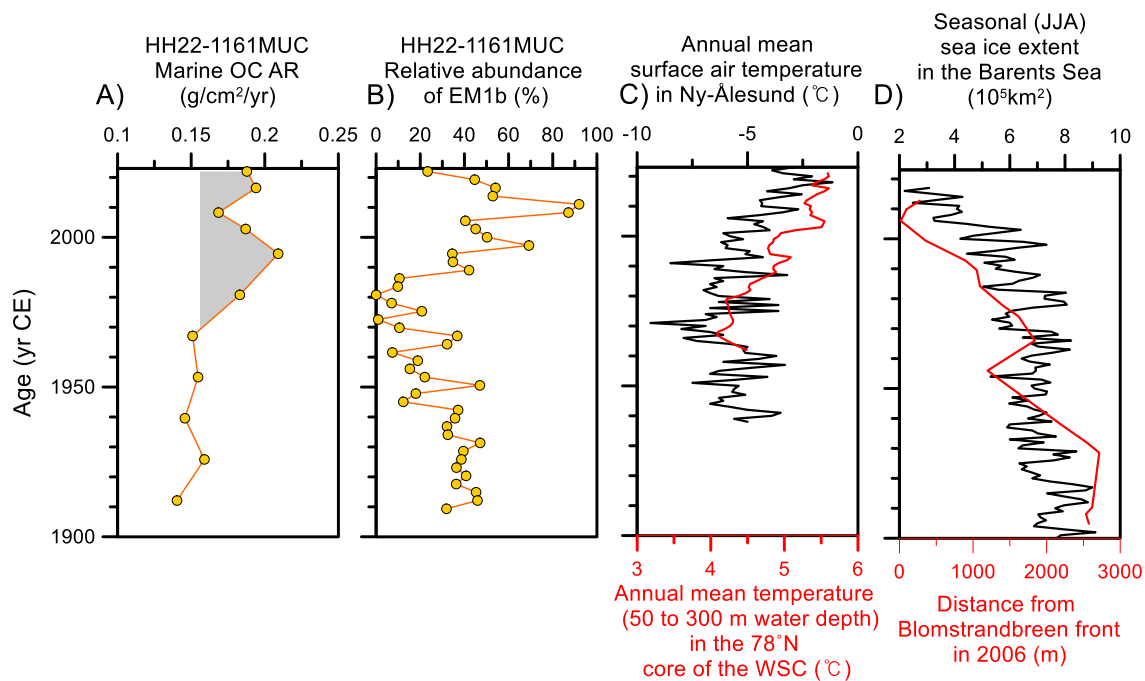
Fig. 10. Age profiles of the accumulation rates (g/cm²/yr) of petrogenic, soil-derived, plant-derived, and marine OC, as determined using Method 1 (based on $\delta^{13}C_{org}$ (‰ VPDB), $\Delta^{14}C_{org}$ (‰), and (Ad/Al)v ratio) and Method 2 (based on $\delta^{13}C_{org}$ (‰ VPDB), $\Delta^{14}C_{org}$ (‰), and lignin phenols (mg/gOC)), for the cores HH23-1058MUC, HH22-1161MUC, and HH22-1159MUC.

Fig. 11. Age profiles of (A) the accumulation rates of marine OC based on Method 2 for core HH22-1161MUC, (B) the relative abundance (%) of EM1b for core HH22-1161MUC, (C) annual mean surface air temperatures (°C) in Ny-Ålesund (black; data from MOSJ, Environmental monitoring of Svalbard and Jan Mayen) and integrated annual mean temperatures (°C) at 50-300 m water depth in the 78°N core of the West Spitsbergen Current (red; data from MOSJ), and (D) seasonal (JJA) sea ice extent in the Barents Sea (black; data from NSIDC; National Snow and Ice Data Center) and the distance from the Blomstrandbreen front in Kongsfjorden in 2006 (red; data from Burton et al., 2016).